PROMOVENDI

The Book of Articles
National Scientific Conference
„Nauka Badania Rozwój”
II edition

www.promovendi.pl
fundacja.promovendi

Organizer:
Promovendi Foundation

Chairman of the Organizing Committee:
Graczyk Andrzej

Members of the Organizing Committee:
Byczkowska Paulina
Firaza Agnieszka
Solarczyk Paweł
Wawrzyniak Dominika

Editor:
Solarczyk Paweł

Promovendi Foundation Publishing

Address:
17/19/28 Kamińskiego st.
90–229 Lodz, Poland

KRS: 0000628361
NIP: 7252139787
REGON: 364954217

e–mail: fundacja@promovendi.pl
www.promovendi.pl

ISBN: 978–83–950109–7–2

Circulation: 35 copies

Warsaw, October 2018

Scientific Committee:

Ph.D. D.Sc. Andrzej Szosland, prof. LUT – Lodz University of Technology
Ph.D. D.Sc. Marta Kadela – Building Research Institute in Warsaw
Ph.D. D.Sc. Jacek Sawicki – Lodz University of Technology
Ph.D. D.Sc. Ryszard Wójcik – The Jacob of Paradies University in Gorzów Wielkopolski
Ph.D. Norbert Kępczak – Lodz University of Technology
Ph.D. Przemysław Kubiak – Lodz University of Technology
Ph.D. Monika Kulisz – Lublin University of Technology
Ph.D. Rafał Miśko – Wroclaw University of Science and Technology
Ph.D. Olga Shtyka – Lodz University of Technology
Ph.D. Aleksandra Perek–Długosz – Technologie Galwaniczne Sp. z o.o.
Ph.D. Kamila Puppel – Warsaw University of Life Sciences
Ph.D. Martyna Rabenda – Skanska S.A.
Ph.D. Radosław Rosik – Lodz University of Technology
Ph.D. Joanna Szala–Bilnik – University of Alabama, US
Ph.D. Robert Święcik – Lodz University of Technology

Reviewers:

Prof. D.Sc. Ph.D. Lech Sitnik – Wroclaw University of Science and Technology
Prof. D.Sc. Ph.D. Waldemar Wołczyński – Institute of Metallurgy and Materials Science Polish Academy of Science in Cracow
Assoc. Prof. D.Sc. Ph.D. Eugeniusz Hotała – Wroclaw University of Science and Technology
Assoc. Prof. D.Sc. Ph.D. Zygmunt Wujek – Koszalin University of Technology
M.D., Ph.D. Agnieszka Bronowicka-Szydełko – Wroclaw Medical University
Ph.D. Marek Wyjadłowski – Wroclaw University of Science and Technology

TABLE OF CONTENTS

MEASUREMENTS IN THE DECOPPERISATION PROCESS

Adam W. Bydałek[1,2*], Szymon Biernat[2], Grzegorz Boczkal[3], Piotr Migas[4], Maciej Wędrychowicz[1]

[1] University of Zielona Góra, Faculty of Mechanical Engineering, Zielona Góra
[2] State Higher Vocational School in Głogów, Głogów
[3] AGH University of Science and Technology, Non-Ferrous Metals Faculty, Kraków
[4] AGH University of Science and Technology, Faculty of Metals Engineering and Industrial Computer Science Affiliation, Kraków
* corresponding author: a.bydalek@iizp.uz.zgora.pl

Abstract:

The article presents selected issues relating to measurements in copper metallurgy, especially in the decoppering process. The study does not show all research methods, but is considered the most important on the way to the knowledge of the effects of coagulation of the metallic phase in the liquid slag. Attention is paid to the effect of copper sedimentation in the slag and the method of its measurement, selected effects of structural analysis were shown. The very important effect of segregation of eutectics in the Cu - O system and the measurement methods was indicated. Authorized database allowing archiving of measurement data was indicated. The presented measurement results are only a fragment of extensive research, which allowed to determine the mechanism of copper separation during the process of decoppering slags.

Keywords:

slag, copper, measurements

Introduction

The process of decoppering the suspension slag in an electric furnace has three different stages. They depend on the prevailing physicochemical phenomena in the process [1-3]. In the first stage, the furnace is filled with the use of spouts (directly from the flash furnace) with liquid slag at a temperature of about 1300 °C, coke and limestone. The duration of this stage is about two hours. During this period, about 80 % of the initial copper value is reduced [3-5]. In this step, the copper content drops to 2 %. The second stage is the longest and lasts 4-5 hours. Copper, iron, arsenic and lead oxides are reduced. There is also sedimentation and coagulation of the reduced metals, which creates a Cu-Fe-Pb alloy. At this stage, the reduction process is very slow and the copper content in the slag decreases to 0.8 % [4,6]. During the last stage, the Cu-Fe-Pb alloy and slag are triggered. It lasts 2-3 hours and the slag temperature is 1350-1380 °C. The final copper content in the slag drops to about 0.5 %. In general, one cycle lasts about 10 hours [1]. Unfortunately, the dropping time of the droplets is so short that it is impossible to reach the equilibrium. What causes that the above-mentioned reactions will continue to occur mainly at the slag-stop boundary [7].

Analysis and testing of coagulation and crystallization of copper in to the slag

Conditions resulting from the difficulty reductions of copper oxides and subsequent entry of reduced metallic phase settling to the bottom of the electric furnace (Figure 1a) were the basis for making analysis and testing of coagulation and crystallization of copper under dynamic conditions. It was decided to take into account and analyses the turbulent movement of the slag during its discovery. The composition of slag suspension is presented in Table 1. Samples were collected during charge of slag into electric furnace. Then collected material was melted in an electric furnace under reducing conditions and cast into a metal mold.

Table 1. The basic chemical composition of the flash furnace slag used for analysis

	Cu	Ag	Pb	Fe	S	As
Slag, % mass	13,64	0,014	3,2	6,24	0,042	0,180

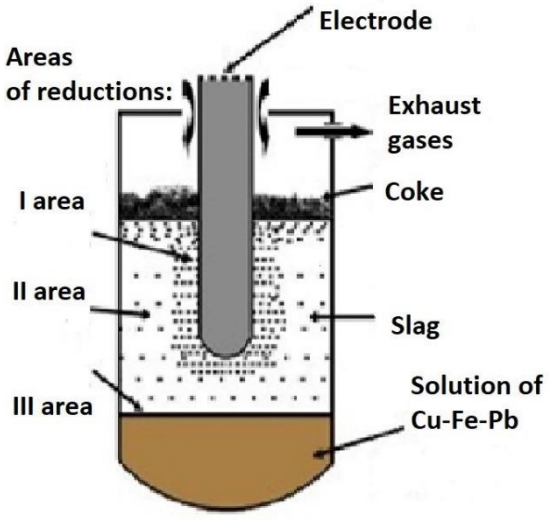

Simplified electrode diagram in a furnace for decontamination of slag

Research position

Figure 1. Description of the scheme of interactions in the electric furnace (a) and tests unit (b)

A stand consisting of a Tammana tubular resistance furnace and a mixer with regulated speed was made for the tests (Figure 1b). Dynamic tests were carried out at 1300 °C. The residence time in the assumed temperature was 20 min. The rotation speed was adjustable from 10 - 30 rpm. The slag from the flash furnace was modified with stimulants and reagents. For the dynamic tests, samples were selected for which, in static conditions, the largest contents of the copper alloy after the reduction process were identified. After cooling the samples reduced under dynamic conditions with the furnace, the obtained products were weighed (slag + metal), then they were ground in a mortar, sieve analysis of obtained fractions was performed subsequently. Figure 2 presents an example of a sample obtained during dynamic coagulation.

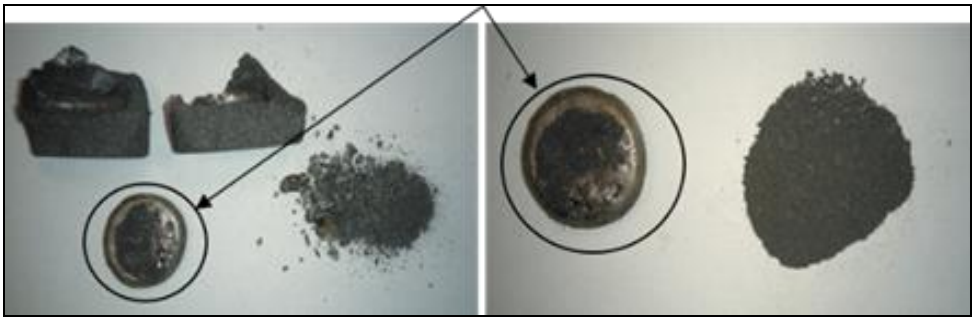

Figure 2. Photographs of the selected sample after dynamic coagulation

Analysis of the structure of slag

The structure shown in Figure 3 is a coat layer between the two test areas, distinguished during the research: area of coagulation of spherical precipitates - mainly Cu-Fe-Pb (area I) and the isolation and crystallization area of metal phase - mainly Cu-Fe-Pb (area II). The following figures show further distinguished areas. Figs 3 and 4 show the structures of area I, highlighting the region Ia - with no fermata-shape phases (Fig. 4), and the area I b – with presence of fermata-shape phases (Fig. 3). Fig. 5 shows results from the structure analyses of area II.

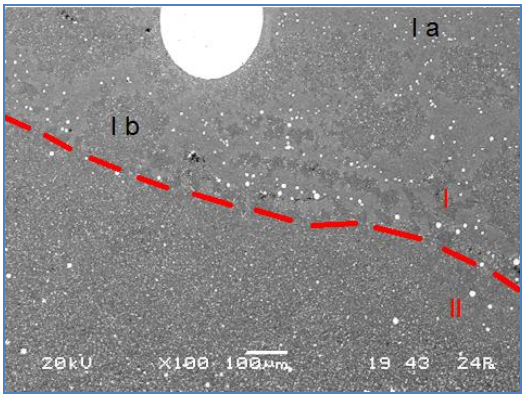

Figure 3. The image of coat layer: I - coagulation area with spherical precipitates of Cu-Fe-Pb slag; I a - no fermata-shape phase, and I b - with the presence of fermata-shape phase; II- precipitates zone and crystallization of a Cu-Fe-Pb from the slag suspension

Fig. 4 shows the structure of the dispersion of fine precipitates rich in silicon, iron, calcium, copper, and large metal separations containing copper, iron and lead – Cu-Fe-Pb alloy. Such structures characterizes with two types of precipitates of Cu-Fe-Pb. First type shows large- 100-150 microns- precipitates separation. Second type – a small flocculent precipitates of Cu-Fe-Pb alloy- is of the size of approx. 5 microns.

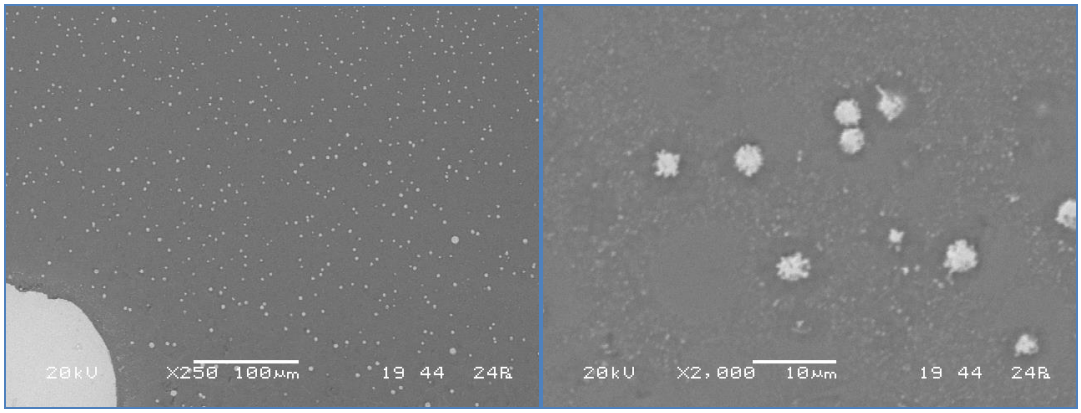

a) b)

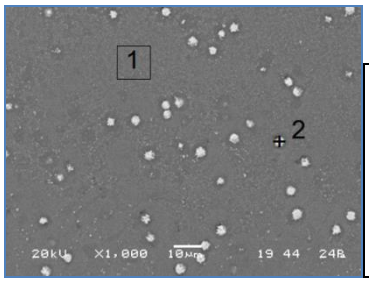

1 - the area with finely disperse precipitates of - silicon, iron, calcium, copper, aluminum, lead, magnesium, potassium, zinc, oxygen

2 - separating metal - copper, iron, lead, aluminum, zinc, calcium, oxygen

c)

Figure 4. The structures of Ia area with the spherical precipitates of Cu-Fe-Pb (according to Fig. 3 - no fermata-shape phase into the slag suspension):
a) slag suspension with separation of the first type,
b) second type of slag suspension with precipitates,
c) the marked areas of analysis and the summary of chemical microanalysis.

The analysis of the chemical composition of areas surrounding these two types of precipitates (Fig. 4) showed differences in composition occurring in immediate environment precipitates. The first type of precipitates showed the following content: Si -20.2% Ca - 15.2% Fe - 10.7% Cu – 6.9%, Pb - 3.4%, K – 1.1%. Meanwhile, the surroundings of precipitates of second type were characterized with: Si - 21.1%, Pb - 13.1% Cu - 9.8%, Ca – 7.8%, Fe - 6.6%, F – 5.5%.

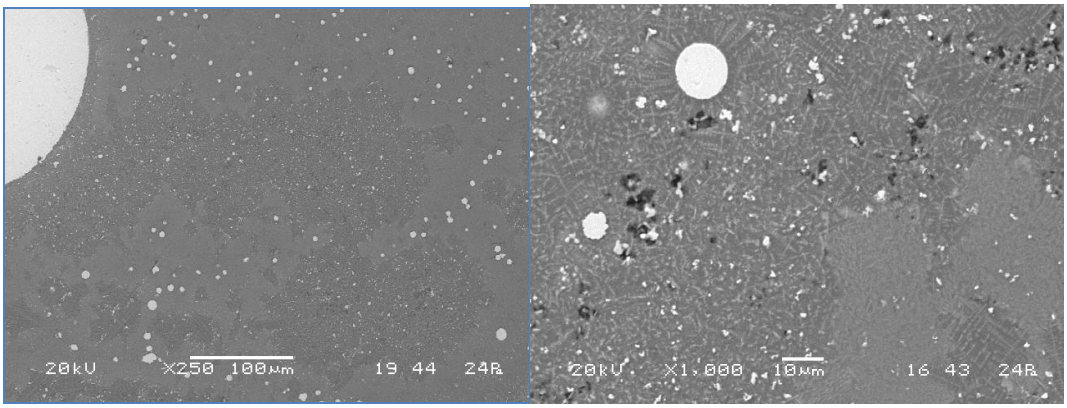

a) b)

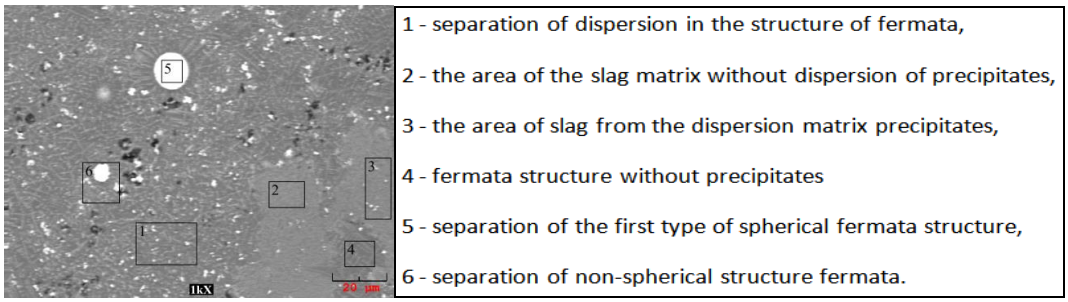

c)

Figure 5. Structure Ib of area with the crystalline precipitates according to Fig. 3 (presence of a suspension slag with the fermata-shape phase):
a) slag suspension with large and small precipitates of the first and second type,
b) the crystal fermata-shape structure of fine separation of the first type, with precipitates of second type being trapped in the spaces between grains,
c) the marked areas of analysis and the summary of chemical microanalysis.

The analysis described above concludes with the thesis for further research: both coagulation and coalescence phenomena, as well as crystallization fermata-shape phases are responsible for the secretion of metallic phase in slag suspension. Thus, it should be possible to take into account the descriptions concerning heterogeneity of concentration that occurs during the process of dendritic crystallization of such multiphase system as slag suspension. It must be assumed that the segregation of components determines the properties of the Cu-Pb-Fe alloy that excretes in the slag slurry. Being in favor of fermata-shape phases, the processes of dissolution of Cu - Fe - Pb precipitates may also be the main causes of changes of viscosity of suspension slag.

Characteristics of the impact of slurry slag from a single-stage process of copper production for the exploitation of ceramic materials

The purpose of the research is to demonstrate the chemical interaction of the slurry slag with the refractory material made of aluminium oxide. After prior grinding in a vibratory crusher and selection to fractions smaller than 0.1 mm, the slurry slag was placed in a ceramic crucible. Slurry slag in the amount of about 80 g was placed in a corundum crucible, and then melted in a resistance furnace in the temperature range from 1200°C to 1380°C every 20°C. After the removal of the studied sample and cooling of the slag the crucible was broken and its fracture was studied macroscopically and microscopically. The slag from the single-stage process of obtaining copper, but also the dusts and the process gases are characterized by high chemical aggressiveness towards the lining of the flash furnace. According to the KGHM monograph in contrast with the classical "Outokumpu" technology, the slurry slag containing about 14 % Cu_2O and having direct contact with the flash furnace lining causes the rapid wear of refractory (ceramic) materials and the deformation of the furnace hearth. In order to confirm the erosive effect of the slag, a test of the effect of the chemical slurry slag on a ceramic material made of Al_2O_3 was carried out. Figures 6 show a macroscopic image of the slurry slag penetrating into the corundum crucible. Figures 7 show an image from a scanning microscope.

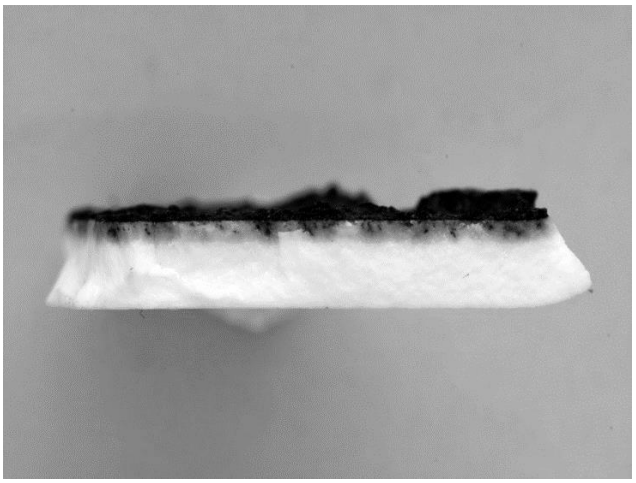

Figure 6. View from the side of the corundum crucible after the measurement of slurry slag at 1360ºC (natural size)

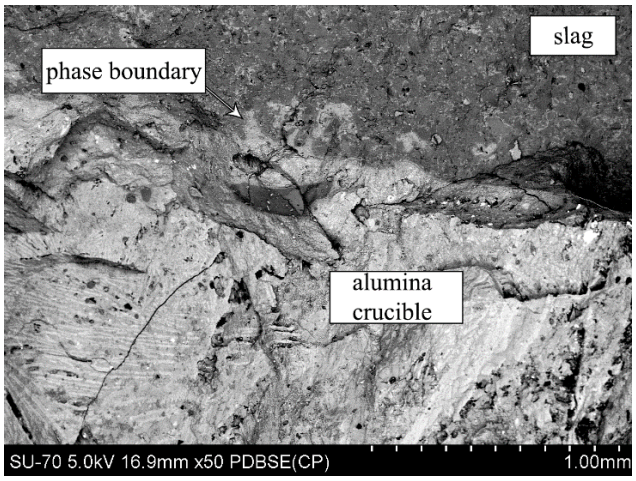

Figure 7. Scanning microscope image of the corundum crucible after the measurements

In all types of flash furnaces the furnace reaction area is among the least durable elements of the furnace and it is decisive in its renovation cycles. Despite the use of the best refractory materials in this area, their durability does not exceed 10 months. The research results presented in the article indicate not only the possibility of dissolution of the ceramic material in the molten slag, but also on the possibility of erosive activity of the slag on that material. Therefore, it is important to conduct further research and works on the development of refractory materials which could allow for extending the cycle of works between the renovations of the flash furnace.

Analysis of the kinetics of cu_2o eutectic crystallization on the process of copper recovery from the slag

During the process of copper recovery from slags in the production of copper, the reduction of oxygen-copper eutectics plays an important role. The second important phenomenon is the coagulation and crystallization of the evolved metallic phase, rich in copper. At temperatures above 1225 ° C in copper with an oxygen content in the range of 10 - 31 atomic%, in the system there is monotectic. At technological temperatures, higher than 1345 ° C, there are two phases of liquid Cu and Cu_2O, which are completely miscible and form only one liquid. Such a liquid was subjected to

the process of crystallization.

A series of studies on the crystallization of Cu-Cu_2O eutectics in slag was presented. The material used for zonal crystallization (the Bridgman method) was highly oxidized copper taken under the slag layer. Copper rods with a diameter of 8 mm were formed from copper, which were then used as a batch for the zone crystallization process. Two atmospheres were distinguished: in a vacuum and without.

It has been shown that the Cu-Cu_2O eutectic found in metallic drops contains two components with different digestibility. It was copper that easily dissolves in nitric acid and an oxide of low reactivity. This allowed for the selective etching of the copper matrix and revealing the morphology of Cu_2O particles - part of eutectic. The observations showed a large morphological diversity of Cu_2O oxide in copper droplets. The sizes of the obtained octahedral particles were similar to those described in the literature. An additional morphological area of Cu_2O eutectics were plates with an edge length of 5 microns. Microstructural studies have shown the effect of the crystallization rate on the forming microstructure. According to the tendency observed during the studies, the low rate of crystallization promotes the formation of the plate structure. It has been found that the increase in eutectic crystallization speed is accompanied by the conversion of the plate → fiber. As a result of the research, a model of transformation of the Cu-Cu_2O eutectic morphology was proposed. The observed dependencies will be of fundamental importance in the processes of detecting post-process slags (Fig. 8-9).

a) 

b) 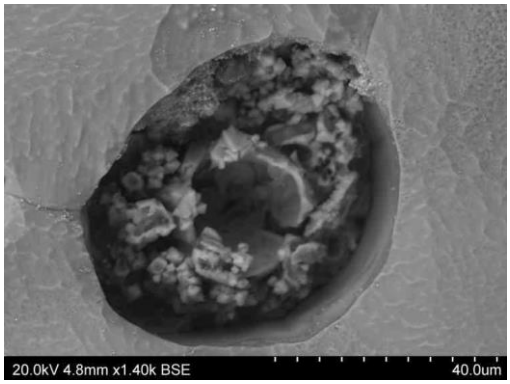

Figure 8. a) Macrostructure of a sample obtained in zonal crystallization in a Bridgman vertical furnace; b) Mixed Cu-Cu_2O eutectics.

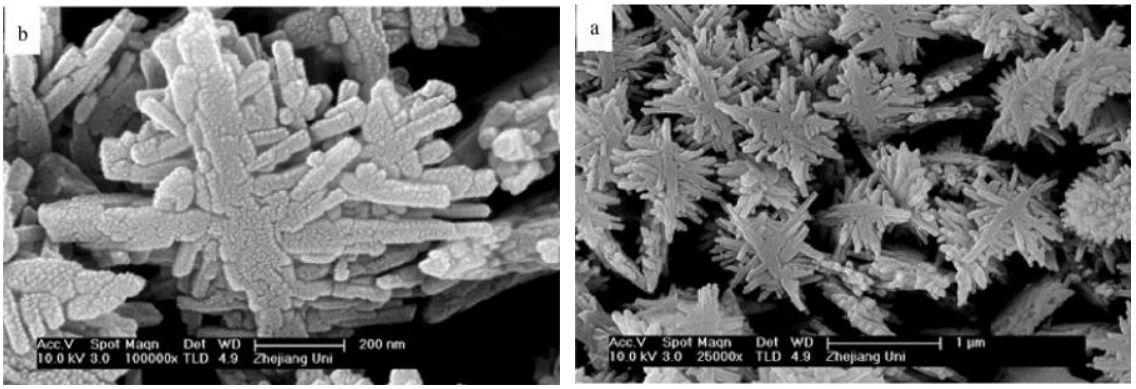

Figure 9. Synthesized Cu_2O nanodendrites

Database of materials for the evaluation of the impact of harmful substances in metallurgical processes

The 21st century is a period of highly developed technologies in which automation, robotics and computerization are applied in almost any industry. New technologies aim to produce products with better quality, in a shorter time, the cheapest costs with the least possible negative impact on the environment. In every modern industrial plant, both a large steelworks and a small foundry, there are a number of devices and machines to achieve those goals. One of the basic elements of advanced manufacturing technologies is today the implementation of an appropriate system that allows the measurement and collection of relevant data, their analysis, and on the basis of developed indicators and algorithms, automatic or semi-automatic control of manufacturing processes. One should pay attention to two integrated areas. One of them is a typically hardware area containing a set of sensors, detectors and probes that collect information and transmit it to the second area, which is the appropriate programming platform able to determine the most appropriate directions.

This study presents an integrated analytical and measurement system for assessing melting conditions for metals and alloys. It consists of two separate parts - hardware and software, which interact in close correlation and exchange data, allowing for taking specific actions to improve production and environmental indicators.

The Slag-Prop Cu database [8] was prepared based of their physical, mechanical and technological properties, collected from their own research and literature. The database combines the information collected over the years of laboratory and industrial research. The material base has been introduced as well as it has the ability to independently add various information regarding the physicochemical properties of certain slag mixtures such as melting point, wetting, surface tension, viscosity, electrical conductivity and others. Each specific property refers to the specific composition of the slag mix. The material database also has experimental data obtained from own research. Not only thermal analysis but also DTA and TG research. On this basis, it will be easy to obtain information on the refining capacity of the selected slag composition. The database can be used not only to search for optimum conditions meeting technological and construction criteria. It may also serve as a basis for setting new scientific orientations. Essential (Fig. 10), therefore, is that the database is openness and can be filled up with new data obtained in laboratory or industrial environments.

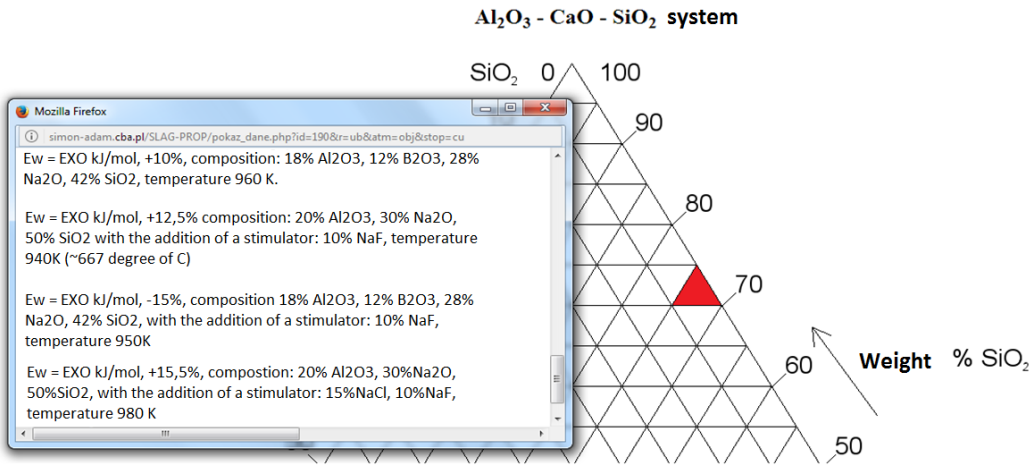

Figure 10. Fragment of slag mix description from Slag - Prop database

In the above figure (Fig. 10), a fragment of the exemplary 3-component mixture - Al_2O_3-CaO-SiO_2, designated with reference number 190 is shown. This number corresponds to the slag mix composition containing 25-30% Al_2O_3, 70-75% SiO_2 and up to 5% CaO. In the next figure (Fig. 5) there is a result of the search of the standard areas of the Al_2O_3 - CaO - SiO_2 slag mix, the weight ratio of which allows the melting point of the system to be below or exactly 1000°C, using the appropriate additives, which were reflected in the database. In this case, 6 areas were found meeting the criteria. The database itself contains a collection of different compositions of slag mixtures. Each layout is represented in the form of a Gibbs graph, which is divided into 400 equal areas. Therefore, the position and use of database applications can greatly facilitate the work of metallurgists, foundries, technologists and scientists themselves.

Acknowledgements

This project was supported by the National Center for Research and Development under Grant No. PBS3/A5/45/2015.

Literature

[1] Elliott, John F. Phase relationships in the pyrometallurgy of copper, Metallurgical Transactions B. vol. 7, pp. 17-33. March 1976.
[2] Zenjiro Asaki, Kinetic Studies of Copper Flash Smelting Furnace and Improvements of its Operation in the Smelters in Japan, Mineral Processing and Extractive Metallurgy Review , Volume 11, Issue 3. 1992.
[3] Mackey P.J., The Physical Chemistry of Copper Smelting Slags-A Review, Canadian Metallurgical Quarterly, Vol. 21, Issue 3. 1982.
[4] Moskalyk, R.R. And Alfantazi, A. M. Corrigendum to "Review of copper pyrometallurgical practice: today and tomorrow". Minerals Engineering. vol. 17, Issue. 1, pp. 103-111. January 2004.

[5] Taskinen P. et al., Oxygen pressure in the Outokumpu flash smelting furnace-Part 1: copper flash smelting settler, Mineral Processing and Extractive Metallurgy, Vol. 110, Issue 2. 2001.
[6] Ahokainen T. et al., Numerical Simulation of the Outokumpu Flash Smelting Furnace Reaction Shaft, Canadian Metallurgical Quarterly, Vol. 37, Issue 3-4. 1998.
[7] Kucharski, M. Effect of thermodynamic and physical properties of flash smelting slags on copper losses during slag cleaning in an electric furnace. Archives of Metallurgy. vol. 32, no. 2, pp. 259-262. 1987.
[8] A. W. Bydałek, S. Biernat, A. Bydałek, P. Schlafka, International Journal of Engineering and Innovative Technology, 4, 5, 186-197, 2014.

ANALYSIS OF LOAD-BEARING CAPACITY OF CYLINDRICAL SHEEL OF STEEL SILO MADE OF CORRUGATED SHEETS SUPPORTED BY A SKIRT

Sławomir Górnicki

Feerum S.A., ul. Okrzei 6, 59 – 225 Chojnów,
corresponding author: s.gornicki@feerum.pl

Abstract:

Paper presents a new solution of steel silos made of corrugated sheets produced by Feerum S.A. company. The paper briefly shows advantages of this solution. Authors show and comment code rulings of calculation load-bearing capacity of vertical stiffeners of steel silo shells made of corrugated sheets. Authors point out a very conservative approach in which rigidity of elastic support of compressed stiffener is calculated. Authors also point out a real risk of bending in stiffeners, which is omitted in code rulings. The correct estimation of the resistance of vertically ribbed silos made of steel corrugated sheets is critical from the standpoint of a structural safety, because most of collapses of silos are related to the exceeding of the resistance of a stiffener. The paper show results of finite element analysis. A linear buckling and non-linear buckling analysis with geometric and material non-linearity were carried out with a perfect and an imperfect silo shell. Authors considered one type of initial geometric wall imperfections. Authors determined factor of load-bearing capacity by taking into account axisymmetric and non-axisymmetric loads imposed by a bulk solid. Results showed that skirt is a critical area of cylindrical shell due to instability. The largest bending in stiffeners occur in transition area. New solution of steel silos reduced material use and difficult technological processes.

Keywords:

steel silos, stiffener, buckling, geometric imperfections, FE analysis

Introduction

Steel silos made of corrugated sheets are commonly used for storage of loose materials, especially of agricultural origin. Storage of cereals in silos allows proper protection of the grain against pollution and rodents, but also allows maintaining optimal storage conditions that allow reducing losses caused by moisture or inadequate temperature. The silo shelling consists of a corrugated metal sheet that transfers tensile latitudinal loads and vertical stiffeners, which in turn transmit the longitudinal (compressive) loads to the foundation. In the current solutions of silos there can be found a few shortcomings, both structural and technological ones. The author in this article presents the results of numerical analysis of the new silo funnel concept, developed as part of the National Centre for Research and Development "NCBiR" research project Development of innovative constructions of lightweight steel and steel-textile silos carried out by FEERUM S.A.

The basic goals that were set in the implementation of the project were primarily to reduce the use of materials, improve the storage conditions of loose units and minimize energy-intensive processes.

Prepared concept of the silo

As part of the research project, the final version of the funnel silo with a diameter of D = 8.6 m was developed. The developed solution resigned from the traditional support of the chamber on steel which was replaced by an apron constituting the extension of the shelling, and the funnel constructions were torn independently. The construction of the conical funnel made it possible to reduce the dustiness of the surroundings. Details of the solution are shown in Figure 1. The silo consists of 22 perimeter carges with a repeatable height hcarga = 1,122 m. The lower part of the shell called the shelling is composed of 6 cargas (Fig. 1a). The thickness of the carged sheets depending on the silo zone is from 0.75 mm to 1.2 mm. The corrugated sheet geometry is shown in Fig. 1b. To transfer the longitudinal compression forces, 18 meridional stiffeners with a hat cross-section (Fig. 1c) were used, in the circumferential spacing every 1.5 m. The stiffeners consist of several sections connected in a continuous manner. Depending on the value of compressive forces, the thickness of individual sections of stiffeners varies from 2 mm to 6 mm in the lower zone of the silo. The stiffeners are connected to the shell by means of high strength bolts. The roof of the silo creates a self-supporting finned cone-shaped shelling with an angle of inclination of 34 °. There is a central hopper as well as a silo discharge. The silo shell and the funnel construction were designed from HX380 steel. The presented solution minimizes energy-intensive processes (welding, galvanizing) and is environmentally unfriendly. In addition, the assembly of the silo structure does not require the use of car lifts.

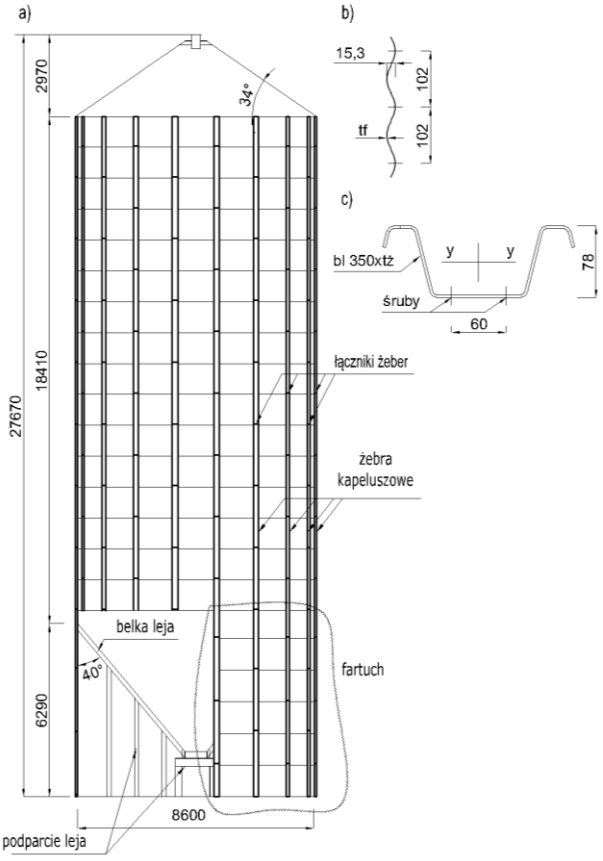

Figure 1. Silo with hopper – cylindrical shell supported by a skirt: a) geometric characteristics of silo, b) geometry of corrugated sheet, c) cross section of sttifener

Buckling capacity of the longitudinal stiffeners of the silo shell

The applicable PN-EN 1993-4-1 design standard proposes two alternative methods for determining the bearing capacity of a single stiffener. In the first method, the stiffness of the sheathing (corrugated sheet) is omitted, treating the stiffeners as an axially compressed rod whose bearing capacity is determined by the formula:

$$N_{b,Rd} = \frac{\chi A_{eff} f_y}{\gamma_{M1}} \tag{1}$$

In the above formula, the effective plastic bearing capacity of the section is multiplied by the buckling coefficient χ, which is determined in accordance with PN-EN 1993-1-1 as with flexural perpendicular to the wall and with the instability curve c, regardless of the stiffener cross-section taken. The buckling length of the stiffener should be taken as between adjacent stiffening rings. If there are no intermediate rings stiffening the shell, the entire height of the shelling should be taken, which at high silos leads to a significant underestimation of the stiffener bearing capacity and is a very uneconomical solution. In the second one proposed, the PN-EN 1993-4-1 standard uses stiffness of the sheath, i.e. corrugated sheet, but the stiffening effect of the stored loose material is

omitted. The stiffener bearing capacity is determined as a smaller value according to the following formula:

$$N_{b,Rd} = \min\left(2\frac{\sqrt{EI_y K}}{\gamma_{M1}}; \frac{A_{eff} f_y}{\gamma_{M1}} \right) \tag{2}$$

In the above formula, in the left-hand expression, K is the rigidity of the elastic substrate, and EIy is the flexural rigidity of the stiffener when bending from the plane tangent to the wall of the silo shell. The second expression is the effective plastic load capacity of the section. The partial safety factor γM1 applied is 1.1. The first expression in formula 2 requires a short comment. This is the result of the solution of the differential equation (formula 3) of the articulated rod on the elastic base.

$$EI\frac{d^4 y}{dx^4} + N\frac{d^2 y}{dx^2} + Ky = 0 \tag{3}$$

where: EI - bending stiffness of the rod, N - axial compressive force, K - rigidity of the elastic foundation, y - horizontal displacement of the compressed rod.

For an articulated support rod at both ends, the bending function is assumed as described in equation 4, which meets all boundary conditions (y0 - amplitude, L - rod height, n - number of buckling half-waves).

$$y = y_0 \sin\left(\frac{n\pi x}{L} \right) \tag{4}$$

The solution of the differential equation consists in finding the minimum critical force Ncrit. After introducing the assumed bending function and its derivatives to the differential equation, the appropriate transformations finally result in the expression of the critical force:

$$N_{crit} = 2\sqrt{EI \cdot K} \tag{5}$$

The standard approach to determining the stiffness of the elastic foundation, in the author's opinion, is very conservative. First of all, in the standard algorithm the curvature of the layer is not taken into account, only the silo sheet is treated as non-curved, which has much lower stiffness. Lowering the stiffness of the elastic foundation K automatically decreases the value of the critical force Ncrit. Attention was also drawn to this in [1], [2], [3]. It should be noted that the PN-EN 1993-4-1 design standard does not address the issue of bending effects of stiffeners, which may occur even in the lower zones of silos [1], [2]. Due to the safety of silo constructions, correct assessment of the bearing capacity of the silo stiffeners is essential, because the vast majority of failure of silos from corrugated sheets results from the exhaustion of the stiffener bearing capacity [3].

Global analysis of the boundary bearing capacity of the silo shelling

The author performed in-depth numerical analyses of the limit bearing capacity of a silo filled with wheat. The calculations were carried out using the Abaqus program. Loads of the shelling and the funnel of the silo from the storage unit were determined based on the PN-EN 1991-4 standard. In order to find the limit load value, the following analyses were carried out:

LBA - linear buckling analysis,

GNA - geometrically non-linear analysis,

GMNA - geometrically and physically non-linear analysis,

GMNIA - geometrically and physically non-linear analysis with imperfections.

The analyses assumed the values of resilience modulus of steel E = 210 GPa and Poisson's ratio v = 0.3. In order to take into account physical non-linearity, an elastic-plastic model of the material without reinforcement was adopted. In non-linear analyses, the Riks method was used to determine the boundary capacity. This method allows the model to pass through the bifurcation point and simulate the behaviour of the structure after losing stability. Four-element S4R elements with reduced integration were used. The total number of finite elements in the silo model was approximately 960,000.

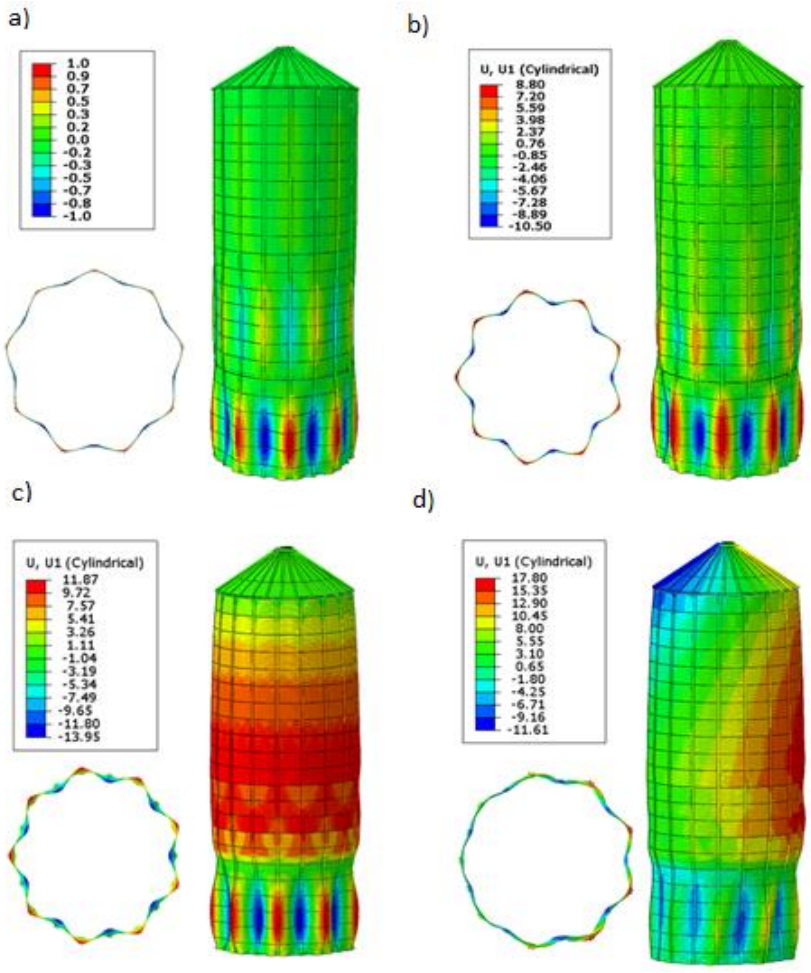

Figure 2. Buckled forms of cylindrical shell: a) analysis LBA, b) analysis GNA (without the axisymmetric horizontal normal stress), c) analysis GNA (with the axisymmetric horizontal normal stress), d) analysis GNA (with the axisymmetric horizontal normal stress and the non-axisymmetric local horizontal normal stress)

First, a linear buckling analysis of the LBA was carried out with the exception of the horizontal pressure phe of the loose agent. The first buckling form was obtained for the boundary capacity multiplier (critical) λLBA = 2.70. In the obtained buckling form of the lower part of the shell (Fig. 2a) 18 buckling half-waves occurred. The stiffeners alternately broke outside and inside the shell. Subsequent buckling forms also included the lower part of the shell, but they had an irregular buckling half-wave system.

In the next step GNA analysis was carried out, which takes into account the effects of higher orders. Three situations were considered. In the first one the horizontal phe pressure was omitted, in the second one the beneficial influence of the horizontal pressure phe was taken into account, and in the third situation the local horizontal pressure ppes was also taken into account. The lowest value of the multiplier λ_{GNA} = 2.47 was obtained for the case with the omission of the influence of the horizontal pressure phe. A buckling form similar to the buckling form from the LBA analysis was obtained (Fig. 2b). Taking into account the horizontal pressure, λ_{GNA} = 2.79 was obtained. The even horizontal pressure has a positive effect on the buckling capacity of the longitudinal stiffners, because this pressure counteracts the resulting buckling half-wave, both latitudinal and meridian, directed to the inside of the shell. Local loads cause the cross-section of the silo shell to ovulate at the place of its impact, thus also causing the bending effects of the stiffeners. For this case, the boundary bearing capacity was λ_{GNA} = 2.65. In each of the analyzed situations, the longitudinal silo stiffeners within the shell buckling (Fig. 2).

Then a GMNA analysis was carried out taking into account material non-linearity. Both symmetrical and local symmetry from the stored unit were taken into account. In this case, the destruction of the shell occurred by plasticizing the stiffenrs at the impact of local pressure, which caused additional flexion effects. The load limit multiplier was λ_{GMNA} = 1.72.

To the task of initial imperfections used symmetrical buckling form obtained from the GNA analysis, for the case with the omission of horizontal pressure. The size of the amplitude of the initial imperfection was determined by the author on the basis of geodetic measurements of meridional stiffeners in analogous construction of silos. Similarly to the GMNA analysis, the symmetric and local pressure of the loose agent was taken into account. The destruction of the silo occurred at the value of the coefficient λ_{GMNIA} = 1.37 and occurred by bending the stiffener within the shell in the direction of the local pressure impact.

Summary

The research carried out allowed us to develop a silo structure corresponding to the customers' needs of Feerum S.A.. A significant reduction in mass has been achieved with a more efficient use of the bearing capacity of individual elements. The author drew attention to the rather conservative norm approaches of determining the load-bearing capacity of meridian silo stiffeners. The rational use of the longitudinal bearing capacity of the silo stiffeners can be obtained by conducting a series of numerical analyzes. The numerical analyzes carried out verified the initial assumptions and showed that the lower part of the shell is the most exposed to loss of stability. In turn, the greatest probability of plastic destruction occurs in the transition zone in which the funnel meets the shell of the silo.

Literature

[1] Hotała E., Kuśnierek M. Skotny Ł., Boniecka J.: Wadliwe połączenia żeber przyczyną awarii stalowych silosów o płaszczach z blach falistych. Materiały XXVII Konferencji Naukowo- Technicznej Awarie Budowlane 2015, Międzyzdroje 20-23 maj 2015, s. 501-508.

[2] Hotała E., Kuśnierek M., Skotny Ł., Boniecka J.: Połączenia pionowych żeber jako słabe miejsca stalowych silosów z blach falistych. Materiały Budowlane, nr 9/2015, s. 102-103.

[3] Iwicki P., Wójcik M., Tejchman J.: Failure of cylindrical steel silos composed of corrugated sheets and columns and repair method using sensitivity analysis. Engineering failure Analysis, nr 18/2011, s. 2064-2083.

Comparison of strength assessment between LEM motorcycle chassis frames using FEM analysis

Piotr Konieczny

Faculty of Mechanical Engineering, Wrocław University of Science and Technology, Wrocław
corresponding author: p.konieczny994@gmail.com

Abstract:

Paper presents comparison of strength assessment between two motorcycle chassis frames of Students Association of Vehicles and Mobile Robots – LEM Falcon and LEM Thunder. The comparison was done using FEM software – Abaqus CAE, that include four different analyse cases: gravity, acceleration, braking and quadruple gravity. The reason of presented article was author desire to check and compare improvements in construction between frames. Paper also shows basic data of the two motorcycles, materials used in the two constructions and their thickness. Also there is presented methodology in preparation shell mode, discrete and calculation models, it's boundary conditions and loads for each frame.

Keywords:

strength assessment, chassis frame, electric motocycle, LEM, FEM

Introduction – LEM Falcon and LEM Thunder

LEM Falcon and LEM Thunder are the light electric motorcycle's projects of Student's Association of Vehicles and Mobile Robots. Both projects in mechanical part include stage of completing the data, completing necessary components, project and calculation of chassis frame, swingarm and linkage system and preparation documentations. The next stage is to make main construction using for example welding technology and then make assembly of whole motorcycle. Each of the motorcycles were made for start in international students competition SmartMoto Challenge that takes place in Barcelona. LEM Falcon is fifth of the LEM motorcycles made in 2017 by students and LEM Thunder is next one made in 2018. Both of motorcycles are shown below in Fig.1 and Fig. 2 below. Also the basic data of each of motorcycle is shown in the Table.1

Figure 1. LEM Falcon
Source: materials of Student's Association of Vehicles and Mobile Robots

Figure 2. LEM Thunder
Source: materials of Student's Association of Vehicles and Mobile Robots

Table 1. The basic parameters of motorcycles

	LEM Falcon	**LEM Thunder**
Power of electric motor „M"	8 kW	30 kW
Engine maximum torque „T"	30 Nm	100 Nm
Motorcycle mass „m"	106 kg	128 kg
Wheel base „l"	1380 mm	1490 mm
Front suspension	FASTACE AKX01RC	WP Xplor 48
Rear damper	DNM MTG-RC 360mm	DNM MTG-RC 360mm

Source: materials of Student's Association of Vehicles and Mobile Robots

Motorcycles chassis frames

Each of the motorcycle's frames contains tubes from the EN AW 6063 T6 of 30 mm diameter and 3 mm thickness, rod of EN AW 6063 T6 for head of frame and sheets of EN AW 7020 T6 of 3,6 and 8 mm thick for ribs. The whole construction was welded using TIG method and additional material - rods from EN AW 5356 for LEM Falcon and EN AW 5356 for LEM Thunder.

The 3D project of frames was created in the SolidWorks software by students. The LEM Thunder chassis frame is improved version of the LEM Falcon frame with changes of the main dimensions in case of different components used in motorcycles: battery, engine and controller. The significant difference between frames lays in the height of the head of the frame. Also the ribs in that area are much extended and create more stiff construction. The frames are presented in the Fig. 3 below. Also Fig. 4 shows the difference between the frames using shell model.

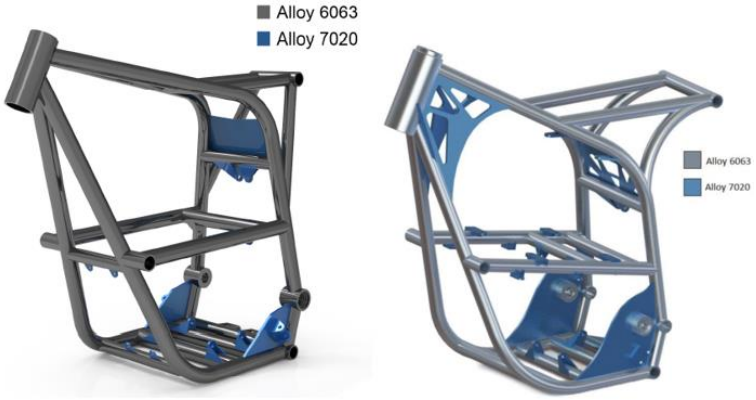

Figure 3. LEM Falcon chassis frame (left) and LEM Thunder chassis frame (right)
Source: materials of Student's Association of Vehicles and Mobile Robots

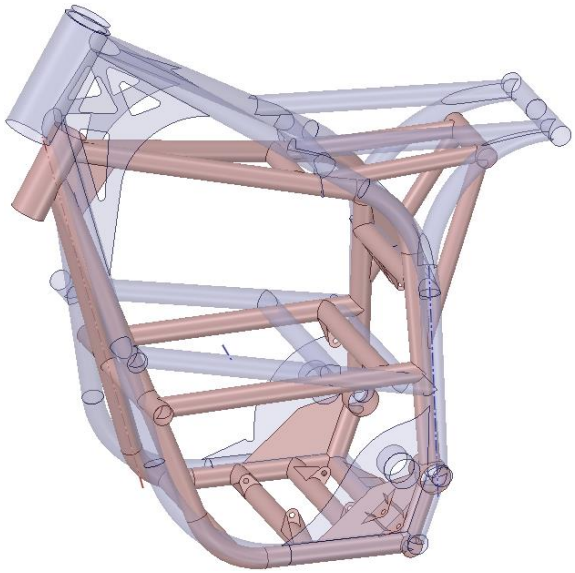

Figure 4. Comparison between frames – LEM Falcon (red) and LEM Thunder (transparent blue)
Source: own materials

Model preparation

In case of use the FEA software – Abaqus CAE, the preparation of the 3D solid model created by students in SolidWorks software occur. Firstly the simplification model of deleting non important fillets, rounds and holes were done. Next from the solid model, the shell model was created. This simplification lets to reduce total number of finite elements in the next stage of discretization model with keeping accurate results in analyses. The significant parts of the whole construction of motorcycle – swingarm, linkage system and handlebar were replaced by rigid link parts. Their main dimensions and points of connection were set according to the 3D assembly model of the motorcycles. Between the parts: swingarm-link, link-shock, shock-frame the revolve kinematic pair were added. Also for front suspension, the cylindrical kinematic pair in head of the frame was created with the parameter of stiffness of two combined typical springs used in motorcycles: 9.6 kN/mm [1]. For the rear suspension, the spring of parameter of stiffness 210 kN/mm [2] was added between frame and shock. Also the COG of 180 cm standing human were set in models and between handlebar and footrests were added springs of stiffness 210 kN/mm to achieve proper influence of driver in analysis cases [3]. The masses of the most influent parts were added as a mass-points: driver 90 kg, engine 20 kg (LEM Falcon) and 10 kg (LEM Thunder), battery 20 kg and 30 kg, controller 7 kg and 9 kg. Beside of the driver, the stiff coupling-kinematic connections to the mounting points of parts were added.

For the discretisation of the shell model of LEM Falcon chassis frame the 90571 linear quadrilateral elements of type S4R and 1831 linear triangular elements of type S3 were created. In case of LEM Thunder frame, the 69764 linear quadrilateral elements of type S4R and 1766 linear triangular elements of type S3 were created. The mesh seed of each frame was set to 4 mm. An example of whole created system of LEM Falcon frame is shown in the Fig.5 below.

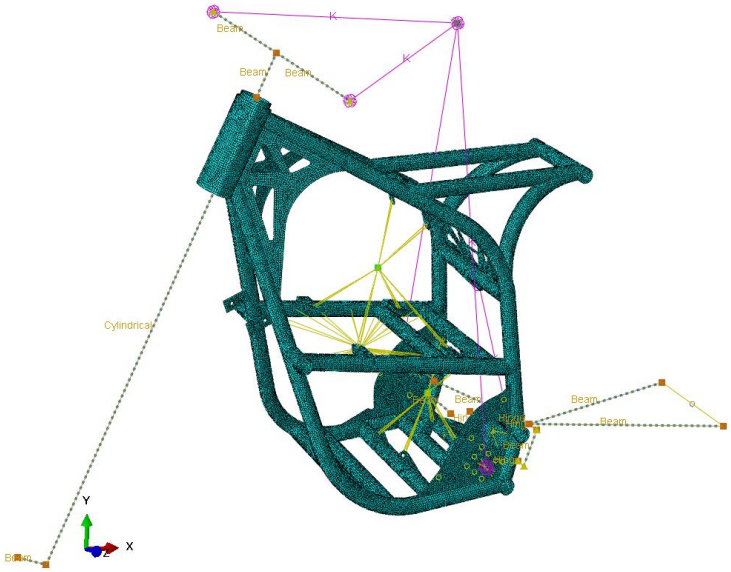

Figure 5. Calculation model of the LEM Falcon chassis frame
Source: own materials

Investigated cases

The constructions were investigated in four cases: gravity, acceleration, braking, quadruple gravity. The last case correspond to the jumping case on the motorcycle. The rest are typical usage situations for the riding. Tab. 2 shows acting loads on the constructions in each cases.

Table 2. Load cases

Case\Load	Gravity [m/s^2]	Longitude acceleration [m/s^2]	Engine torque [Nm]	Chain force [N]
LEM Falcon				
Gravity	9.81	-	-	-
Acceleration	9.81	9.81	30	2000
Braking	9.81	-9.81	-	-
Quadruple gravity	39.24	-	-	-
LEM Thunder				
Gravity	9.81	-	-	-
Acceleration	9.81	9.81	100	3056 [4]
Braking	9.81	-9.81	-	-
Quadruple gravity	39.24	-	-	-

Source: own materials

The boundary conditions were also added in the points of attachment between the wheels and construction. Tab. 3 shows constrained degrees of freedom of each points in cases. The coordination system was set according to the Fig. 5.

Table 3. Boundary conditions

Case\Point	**Front wheel**	**Rear wheel**
Gravity	TXYZ	TYZ RXY
Acceleration	TYZ RXY	TXYZ
Braking	TXYZ	TYZ RXY
Quadruple gravity	TXYZ	TYZ RXY

Source: own materials

For each construction the safety factor and maximum allowable stresses level according to Huber-Mises was set. Coefficient of safety contains [5,6]:

- $FS_{material} = 1.1$ – for examined materials,
- $FS_{stress} = 1.05$ – in case of load cases,
- $FS_{geometry} = 1.1$ – for big geometrical tolerances because of welding frame,
- $FS_{failure\ analysis} = 1$ – for prototype motorcycle,

- $FS_{reliability} = 1.3$ – in case of important role of the part in whole construction.

The maximum allowable stresses was set according to the formula shown below. For the yield strength, the value of 170 MPa for EN AW 6063 T6 and 280 MPa for EN AW 7020 T6 was set [7].

$$FS = FS_{material} * FS_{stress} * FS_{geometry} * FS_{failure\ analysis} * FS_{reliability} \quad (1)$$

$$\sigma_{\min(EN\ AW6063\ T6)} = \frac{Re_{AW\ 6063}}{FS} = \frac{170}{1.65} = 103\ MPa \quad (2)$$

$$\sigma_{\min(EN\ AW6063\ T6)} = \frac{Re_{AW\ 6063}}{FS} = \frac{280}{1.65} = 160.7\ MPa \quad (3)$$

Analysis results

The results of the most concentrated stress areas according to the Huber-Mises stresses between the cases are presented in the Tab. 4 below. The investigated areas are shown in Fig. 6. Also some examples of results are presented in the Fig.7-9 below.

Table 4. Analysed cases stresses [MPa] according do Huber-Mises

Case\Area	1: Frame's head	2: Frame-damper	3:Frame-shock	4: Footrest ribs
LEM Falcon				
Gravity	27.1	22.3	22.1	26
Acceleration	32.1	30.3	30.0	53.5
Braking	74.1	11.2	5.3	10.0
Quadruple gravity	65.3	68.1	85.1	106.1
LEM Thunder				
Gravity	12.4	27.1	27.4	28.9
Acceleration	16.3	49.3	37.1	41.7
Braking	42.8	14.4	4.8	6.6
Quadruple gravity	39.1	97.2	92.4	92.9

Source: own materials

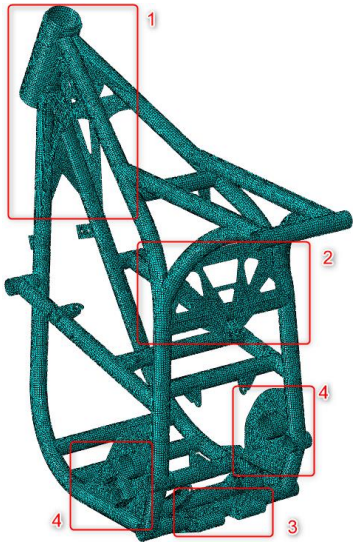

Figure 6. Most concentrated areas of stresses
Source: own materials

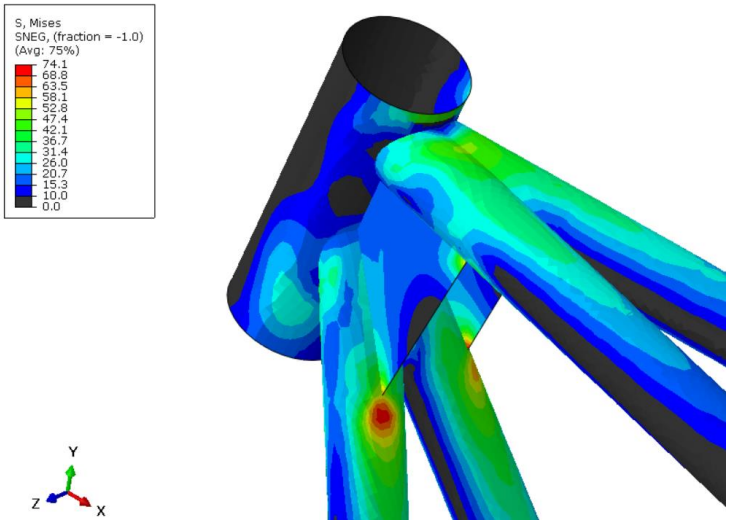

Figure 7. Stresses according to Huber-Mises, LEM Falcon – braking case
Source: own materials

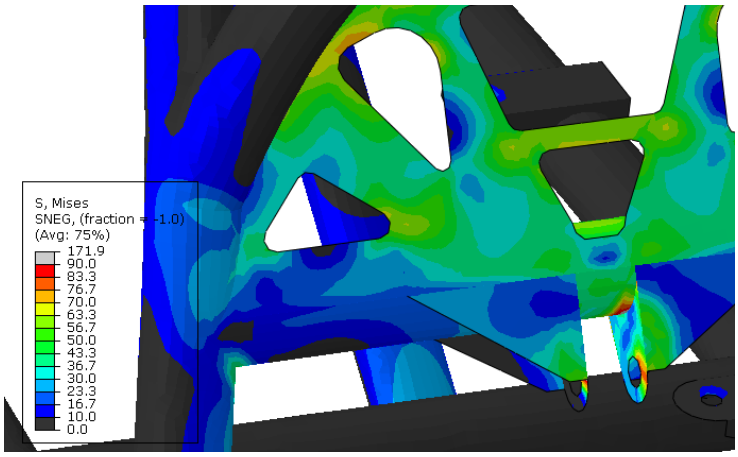

Figure 8. Stresses according to Huber-Mises, LEM Thunder – quadruple gravity case
Source: own materials

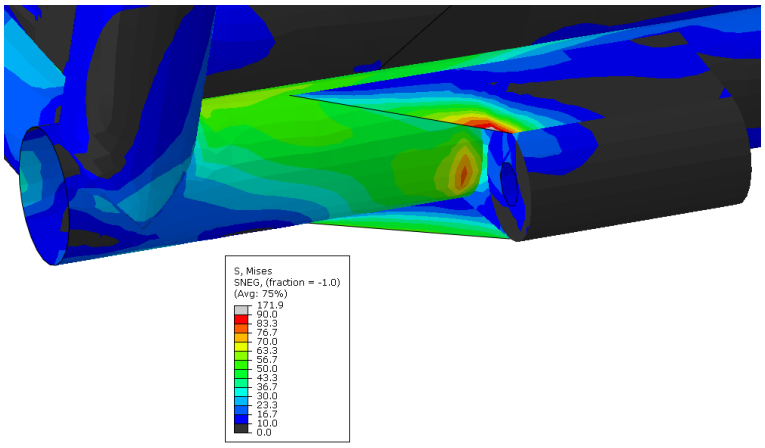

Figure 9. Stresses according to Huber-Mises, LEM Thunder – quadruple gravity case
Source: own materials

Conclusions

Both of the frames were tested in the same four analysis cases. For LEM Falcon frame the region of the head is most loaded in the case of braking. It could be possible to be most dangerous case due to the fatigue strength of the frame. Also greater stresses according to the Huber-Mises occur in the areas of frame-shock connection and area nearby footsteps ribs in the quadruple case. The stresses did not exceed maximum allowable regions. Also this case correspond to the jumping of the motorcycle which did not occur as often as braking case.
The LEM Thunder frame has lower values of the stresses in cases comparing to the LEM Falcon. The higher location of the head of frame forced to make head more stiff and add larger ribs. This helped chassis in the strength assessment of the braking case at the cost of higher mass of construction. However similar design features of connections frame-shock and frame-damper in two frames also in LEM Thunder leaves this areas to be the most loaded in the whole construction. An example of results of quadruple gravity proofs that fact.
The conducted simulations could be a base to the fatigue assessment calculations of the frames in the future. Also an improvement connection of frame to the shock and frame to the damper should be considered in the next constructions.

Literature

[1] Źródło internetowe:
http://www.q-springs.com/wp-content/uploads/motocross-springs-KTM.pdf
[2] Źródło internetowe:
http://www.sport-toys.com/DNM-MTG-RC-360mm-REAR-SHOCK
[3] Praca magisterska:
P.Konieczny, *Dynamic analysis of the motorcycle and driver movement during overcoming obstacles*, Politechnika Wrocławska, 2018
[4] Referat konferencyjny:
P. Konieczny, W. Pawlak, *Dobór parametrów przekładni napędu do crossowego*

motocykla elektrycznego na przykładzie LEM Thunder, 42. Studencka Konferencja Naukowa, Częstochowa, 7 czerwca 2018

[5] Monografia:
D.G. Ullman, The Mechanical Design Process, Second Edition, Ohio 1997, s. 314-317,

[6] Rozdział w monografii:
P. Konieczny, *Dobór geometrii subramy do motocykla elektrycznego z uwzględnieniem obliczeń wytrzymałościowych,* Interdyscyplinarność badań naukowych 2018, Wrocław 2018

[7] Źródło internetowe:
http://www.sebros.eu

ACTIVE AND PASSIVE PRESSURE IN THE ASHES UNDER THE CLIMATE INFLUENCE

Janusz Kozubal, Piotr Wyborski*

Faculty of Civil Engineering, Wrocław University of Technology,
Wybrzeże S. Wyspiańskiego 27, 50-370 Wrocław, Poland
* corresponding author: piotr.wyborski@student.pwr.edu.pl

Abstract:

In the homogeneous material of ground we were observed strong climate influence in its strength and mechanical parameters. Particularly clearly this phenomenon is visible in the case of ashes. They are occurring in large quantities and they are posing many threats for the stability of deep excavations. Frequent case when the water volume of infiltration or evaporation on at surface are caused important changes of saturation inside substrate. In this paper was indicated the method of extended analytical determination of earth pressure value. Authors presented computational cases for illustrating gains of earth pressure in comparision to the classical approach that did not take into account the influence of negative pore pressure in the ground. The basical concept of determining the effective suction in vertical profile was spoted and described. The impact on soil strength characteristics was mesured and it was presented in often used practical aspects of unsaturated soil mechanics.

Keywords:

active earth pressure, passive earth pressure, ashes, suction profile, unsaturated soil

Introduction

Owing to the Digital Revolution, also known as the Third Industrial Revolution, we are witnessing the development of all fields of science. High-power computers and numerical methods have enabled the rapid development of geotechnics. Thanks to these tools, we are able to analyze and understand the phenomena occurring in between construction and ground with complex dependencies between soil and enviroment. One of phenomena which is describing these problems is matric suction connected with apparent cohesion and possible occur of vertical craks. The apparent cohesion is particularly visible in dense porous soils, it is espcecially noticed in ashes and slags, although they are characterized by a large variety of parameters [1]. Along with the increase in ecological awareness, ashes and slags are increasingly used in earthworks, for example due to the possibility of mineral resources being depleted.

The paper is a proposition of the method to calculate the value of apparent cohesion and earth pressure. The geotechnical parameters have been adopted on the basis of Zydroń's and Gruchot's research [2]. In terms of granulometry, ashes and slags resemble silty sand. The first step was determined the flow in the soil to calculate the matric suction profile. For this purpose,

the Lu and Griffiths [3] model was used, taking into account climatic data for the construction site. Lot of empirical formulas were checked and as developed by researchers as [4], [5], [6], [7]. For further calculations the formula proposed by Fredlund and Rahardjo [8] was selected, due to its simplicity. Knowing the values of matric suction, apparent cohesion was calculated. The apparent cohesion was taken into account when calculating the earth pressure. In the second step the influence of apparent cohesion for earth pressure value was considerabled. Despite having many numerical programs such as Abaqus or Plaxis, these calculations in geotechnical issues are associated with a large amount of time consumption, so it is useful to create calculative analytical models to solve engineering problems.

The profile of matric suction

The soil that is the subject of research is in an unsaturated state. Such soil is treated as a three-phase material, where air and water is in the pores of the soil. The unsaturated soil has a negative pore pressure, which can be described by matric suction. This phenomenon causes the mutual attraction of soil molecules, which is determined by means of apparent coherence. The apparent cohesion should be taken into account of calculating the pressure of the ground.

The method used for the calculation of the matric suction value in vertical profile is described by Lu and Griffiths in [3].

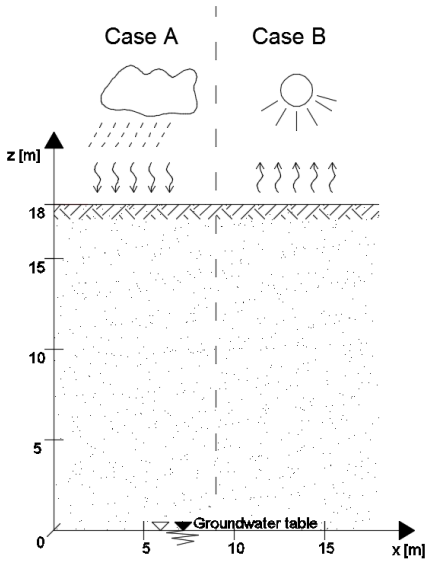

Figure 1. Scheme of adopted coordinate system
Source: Own content

In the Cartesian's coordinate system, where positive coordinates are upward were assumed, in accordance with Figure 1, in the direction - from the groundwater table to the ground level, Darcy's law for unsaturated soils is as follows:

$$q = -k\left(\frac{d\Psi}{dz} + 1\right) \tag{1}$$

where:
q - vertical flow rate [m/s],

k – hydraulic conductivity for unsaturated soils depending on matric suction,
z – vertical coordinate,
Ψ – matric suction in meters of water column [m].

$$\Psi = -\frac{(u_a - u_w)}{\gamma_w} = -\frac{\psi}{\gamma_w} \tag{2}$$

where:
γ_w – specific weight of water [kN/m^3],
u_a – air pressure in the pores [kPa],
u_w – water pressure in the pores [kPa],
ψ – matric suction [kPa]

In order to calculate the hydraulic conductivity for unsaturated soils, the Gartner model was used:

$$k = k_s e^{\beta\Psi} \tag{3}$$

where:
k_s – hydraulic conductivity for fully saturated soils [m/s],
β – pore size distribution parameter.

$$\beta = \gamma_w \alpha \tag{4}$$

where:
α – inverse of the air entry pressure in the ground pores [kPa^{-1}]

By means of equations (1) and (3) and the boundary condition that the matric suction at the groundwater table ($z = 0$) is zero, the following analytical solution describing the value of matric suction in the vertical profiles can be obtained.
Substitution of equation (3) to equation (1) leads to differentia equation:

$$q = -k_s e^{\beta\Psi}\left(\frac{d\Psi}{dz} + 1\right) \tag{5}$$

$$-\frac{q}{k_s}dz = e^{\beta\Psi}d\Psi + e^{\beta\Psi}dz \tag{6}$$

$$dz = -\frac{e^{\beta\Psi}d\Psi}{e^{\beta\Psi} + \frac{q}{k_s}} = -\frac{1}{\beta}\frac{d\left(e^{\beta\Psi} + \frac{q}{k_s}\right)}{e^{\beta\Psi} + \frac{q}{k_s}} \tag{7}$$

Integration of the equation (7) with taking into account the boundary condition (matric suction is zero at the groundwater table) leads to:

$$\int_0^z dz = -\frac{1}{\beta}\int_0^{\Psi}\frac{d\left(e^{\beta\Psi} + \frac{q}{k_s}\right)}{e^{\beta\Psi} + \frac{q}{k_s}} \tag{8}$$

$$-\beta z = ln\frac{e^{\beta\Psi} + \frac{q}{k_s}}{1 + \frac{q}{k_s}} \quad (9)$$

$$\Psi = \frac{1}{\beta} ln\left[\left(1 + \frac{q}{k_s}\right)e^{-\beta z} - \frac{q}{k_s}\right] \quad (10)$$

Substituting equations (2) and (4) to equation (10) leads to a formula for matric pressure [kPa]:

$$\psi = \frac{-1}{\alpha} ln\left[\left(1 + \frac{q}{k_s}\right)e^{-\gamma_w \alpha z} - \frac{q}{k_s}\right] \quad (11)$$

Using the above equations, we can obtain the size distribution of the matrix suction in the vertical profile. The necessary coefficients are included in table 2.

Table 1. Range of soil parameters for various soils

Soil type	n [-]	$\alpha\ [kPa^{-1}]$	S_r [%]	$k_s\ [m/s]$
Sand	4 – 8,5	0,1 – 0,5	5 – 10	$10^{-2} - 10^{-5}$
Silt	2 – 4	0,01 – 0,1	8 – 15	$10^{-6} - 10^{-9}$
Clay	1,1 – 2,5	0,001 – 0,01	10 – 20	$10^{-9} - 10^{-13}$

Source: [3]

The next step is to determine the water flow in the ground. For this purpose, climatic data from the closest meteorological station were used. Table 3 presents climatic data for the selected weather station in Kielce. Table was prepared on the basis of [9], [10].

Table 2. Climatic data for the weather station in Kielce

Month	Average monthly temperature [C°]	Average monthly relative humidity [%]	Average monthly specific humidity [g/kg]	Averege of the total solar radiation intensity [W/m²]	Amount of the total solar radiation intensity $[w/m^2]$	Total monthly rainfall [mm]
January	-1,25	85,73	3,22	17,36	12912,70	36,8
February	-2,10	83,09	2,96	18,34	12324,70	30,0
March	0,45	78,05	3,21	22,25	16554,80	40,3
April	7,52	75,23	4,98	23,58	16979,10	37,4
May	12,96	72,22	6,72	23,45	17449,80	61,7
June	15,20	73,70	7,95	26,50	19082,40	71,0
July	17,68	75,80	9,75	23,78	17691,20	89,5
August	16,04	77,92	9,02	18,74	13938,90	73,6
September	12,69	82,92	7,80	22,64	16301,70	55,5
October	8,52	86,25	6,15	17,52	13031,60	36,7
November	2,33	88,81	4,23	16,03	11540,20	43,7
December	0,04	88,93	3,63	16,66	12392,50	41,5
					Annual amount of rainfall [mm]	617,7

Source: [9] and [10]

The maximum value of the total monthly rainfalls (July – 89,5 mm) was assumed to be the maximum value of infiltration. An indirect flow rate at infiltration was taken as the annual amount of rainfall. Evaporation flow values were assumed equal to the infiltration value.

Table 3. Range of infiltration (-) or evaporation (+) rates

flux [m/s]	flux [mm/day]	flux [m/year]
$-3{,}34 * 10^{-8}$	-2,887	-1,054
$-1{,}96 * 10^{-8}$	-1,692	-0,618
0	0	0
$1{,}96 * 10^{-8}$	1,692	0,618
$3{,}34 * 10^{-8}$	2,887	1,054

Source: Own calculations

The material in which the calculations will be carried out is ashes and slags. Geotechnical parameters have been determined supported on the paper [2]. The geotechnical parameters needed to establish apparent cohesion are shown below:

c (total cohesion) – $0\ kPa$

ϕ'(angle of repose) – $33°$

k_s(hydraulic conductivity) – $3.10 * 10^{-7}\ m/s$

γ (specific weight) – $14.57\ kN/m^3$

$\alpha = 0{,}05$ – Due to the high content of the silt fraction (34.9%, according to [2]) and the value of the hydraulic conductivity, the value from the range for silt was assumed.

The authors of the article [3], for practical reasons, propose to assume the value of matric suction equal to zero if the logarithmic value in equation (10) or (11) is less than zero (breakpoints in Fig. 2 and Fig. 3). The results of the research carried out on unsaturated soils [11] show that the matric suction values increase to a certain maximum value characteristic for a given type of soil. Therefore, it was assumed that the soil reaches the maximum calculated matrix suction value for a given flow in places where the logarithmic value in equation (11) is less than zero.

The values of matric suction are illustrated in the graph below.

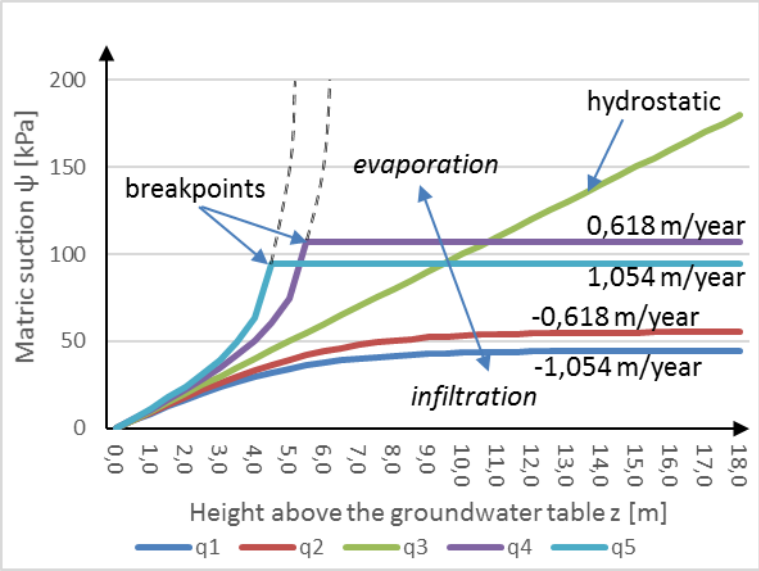

Figure 2. The Values of matric suction in the vertical profile
Source: Own calculations

The influence of matric suction on soil strength parameters

There are several formulas for apparent cohesion, all give similar results. In this paper was used the equation proposed by Fredlund and Rahardjo [8], which modifies the Coulomb-Mohr yield surface by changing cohesion as in formula:

$$c = c' + \psi * tan\phi^b \tag{12}$$

where:
c – apparent cohesion,
c' – effective cohesion,
ϕ^b – angle inclination a rate of increase in shear strength with respect to a change matric suction.

The characteristic values of parameters for wide soil types are shown in table 6 via [8].

Table 4. Experimental values measured for ϕ^b

Soil type	$c'[kPa]$	$\phi'[°]$	$\phi^b[°]$
Boulder clay; $w = 11{,}6\%$,	9,6	27,3	21,7
Dhanauri clay: $w = 22{,}2\%, \rho_d = 1580\ kg/m^3$	37,3	28,5	16,2
Dhanauri clay : $w = 22{,}2\%, \rho_d = 1478\ kg/m^3$	20,3	29,0	12,6
Dhanauri clay: $w = 22{,}2\%, \rho_d = 1580\ kg/m^3$	15,5	28,5	22,6
Dhanauri clay: $w = 22{,}2\%, \rho_d = 1478\ kg/m^3$	11,3	29,0	16,5
Madrid grey clay: $w = 29\%$	23,7	$22{,}5^a$	16,1
Tappen – Notch Hill silt: $w = 21{,}5\%, \rho_d = 1590\ kg/m^3$	0,0	35,0	16,0

^{a} – *average value*

Source: [8]

The values of parameters for silt were established:

- $\phi^b = 16°$

- $c = c' + \psi * tan\phi^b = 0 + \psi \tan 16$

The values of apparent cohesion in the vertical profile are illustrated in the graph below.

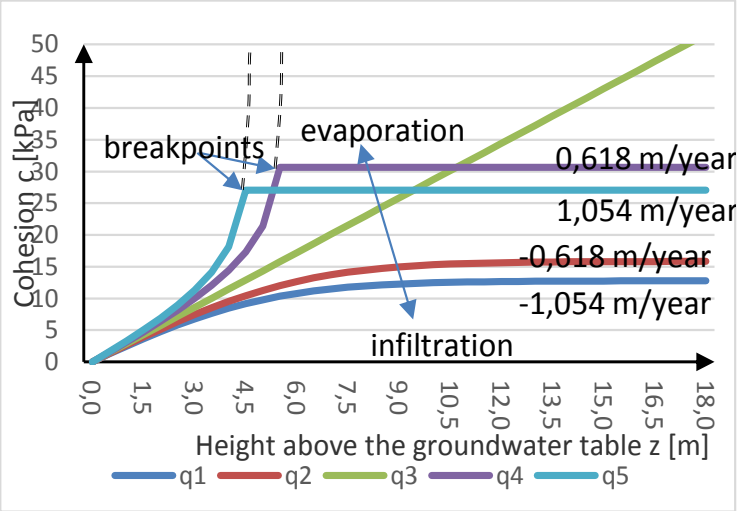

Figure 3. Cohesion values in the vertical profile
Source: Own calculations

Apparent active and passive earth pressure

The apparent active earth pressure e_a and apparent passive earth pressure e_p were calculated according to the extandent Rankine's theory:

$$e_a = \sigma_z K_a - 2(c' + \psi * tan\phi^b)\sqrt{K_a} \tag{13}$$

$$e_p = \sigma_z K_p + 2(c' + \psi * tan\phi^b)\sqrt{K_p} \tag{14}$$

where:
σ_z – vertical geostatic stress, where $\sigma_z = \gamma h$ [kPa],
h – depth below ground level [m],
K_a – coefficient of active earth pressure [-],
K_p – coefficient of passive earth pressure [-],

In the case under consideration, the coefficient of active earth pressure is given by:

$$K_a = \tan^2\left(45° - \frac{\phi}{2}\right) \tag{15}$$

In the case under consideration, the coefficient of passive earth pressure is given by:

$$K_p = \tan^2\left(45° + \frac{\phi}{2}\right) \tag{16}$$

Case study

It was assumed that the backfill is loaded with a distributed load: $Q = 15\ kN/m^2$.The following cases have been adopted for the calculation:

A - the highest flow at infiltration,

B - the highest flow at evaporation.

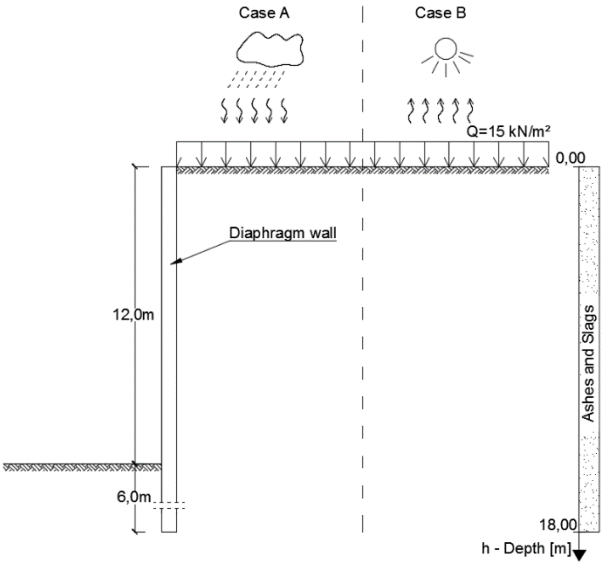

Figure 4. Construction scheme
Source: Own content

According to [12], the Design Approach 2 was used. The active earth pressure was treated as a unfavorable constant actions and was multiplied by $\gamma_G = 1{,}35$. The passive earth pressure was treated as a favorable constant action, and thus the coefficient is $\gamma_G = 1{,}0$. Load on the backfill was taken as an unfavorable changeable load, which was multiplied by $\gamma_Q = 1{,}5$.

It was assumed that the excavation will be excavated to a depth of 12 meters below ground level.

Case A

The earth pressure values for the case of maximum infiltration are illustrated in the graph below.

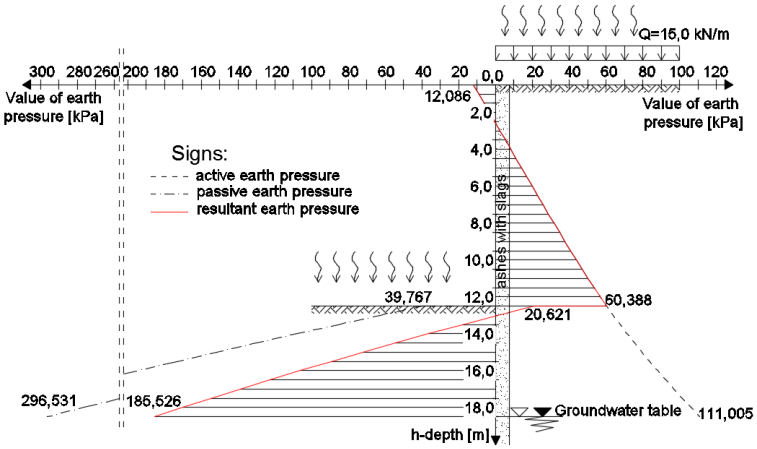

Figure 5. Earth pressure values for the case A
Source: Own calculations

Case B

The earth pressure values for the case of maximum evaporation are illustrated in the graph below.

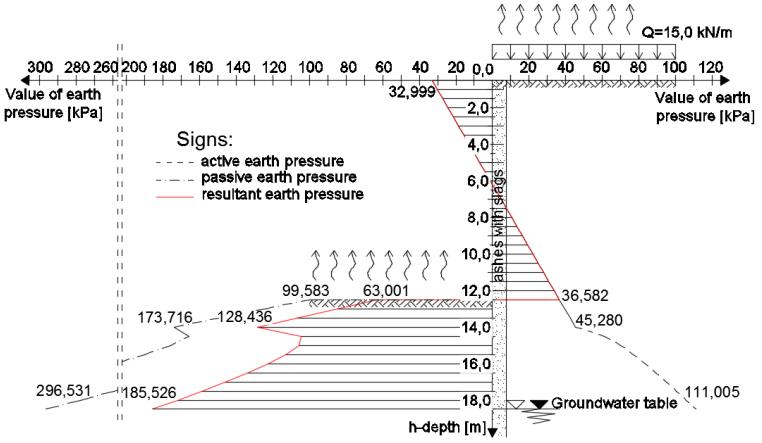

Figure 6. Earth pressure values for the case B
Source: Own calculations

Results and closing remarks

On the basis of the results obtained, the reason for calculation apparent cohesion is visible. Even taking account of the negative scenario (maximum infiltration) a relatively high value of apparent cohesion was obtained and thus the earth pressure values are significantly different from those calculated using classical methods. Considering the apparent cohesion when designing the building construction, we can achieve noticeable advantages.

From the results obtained, one can notice a large difference between cohesion values at maximum evaporation and maximum infiltration. When designing, it is recommended to use the smallest apparent cohesion values, because applying a higher value in connection with unexpected rainfall may result in a building disaster, because the values of apparent cohesion are decreasing, so the values of active earth pressures increase and the values of passive earth pressures decrease. In this case it is more difficult to meet the conditions of material strength and structural stability.

On the basis of the results obtained we can concluded that the climatic conditions have a significant influence on the strength and mechanical parameters (for example shear strength).The paper shows the necessity of appropriate modification of the climate impact on the object and, in a sense, the management of the building development period from the seasonal weather forecasts, so as to optimally use them. All shown formulas and proceduresare are suitable for numerical modeling.

Literature

[1] M. Kadela, M. Gwóźdź-Lasoń, I. Dudko-Pawłowska, *Parametry geotechniczne wybranych odpadów kopalnianych i hutmiczych,* Zeszyty Naukowe Instytutu Gospodarki Surowcami Mineralnymi i Energią Polskiej Akademii Nauk, (2016), Vol. 94, 229-242.

[2] T. Zydroń, A. T. Gruchot, *Wpływ wilgotności i zagęszczenia na wytrzymałość na ścinanie popioło-żużli i stateczność budowanych z nich nasypów,* Annual Set The Envirionment Protection, (2014), Vol. 16, 498-518.

[3] Ning Lu, D. V. Griffiths, *Profiles of Steady-State Suction Stress in Unsaturated Soils,* Journal of Geotechnical and Geoenvironmental Engineering, (2004), Vol. 130, No. 10.

[4] L. Montrasio, R.Valentino, *A model for triggering mechanisms of shallow landslides,* Natural Hazards and Earth System Sciences, (2008), Vol. 8, 1149-1159.

[5] N. Khalili, M. H. Khabbaz, *A unique relationship for χ for the determination of the shear strength of unsaturated soils,* Géotechnique, (1998), Vol. 48, 681-687.

[6] S. K. Vanapalli, D. G. Fredlund, D. E. Pufahl, A. W. Clifton, *Model for the prediction of shear strength with respect to soil suction,* Canadian Geotechnical Journal, (1996), Vol. 33, 379-392.

[7] Y. Matsushi, Y. Matsukura, *Cohesion of Unsaturated Residual Soils as a Function of Volumetric Water Content,* Bulletin of Engineering Geology and the Environment, (2006), Vol. 65, 449-455.

[8] D. G. Fredlund, H. Rahardjo, M. D. Fredlund, *Unsaturated Soil Mechanics in Engineering Practise,* Hoboken, New Jersey: John Wiley & Sons, Inc, 2012.

[9] *Dane klimatyczne,* http://www.pogodynka.pl/polska/daneklimatyczne/, 22.04.2018.

[10] *Dane do obliczeń energetycznych budynków,* https://www.miir.gov.pl/strony/zadania/budownictwo/charakterystyka-energetyczna-budynkow/dane-do-obliczen-energetycznych-budynkow-1/, 22.04.2018

[11] B. Grabowska-Olszewska, *Geologia stosowana Właściwości gruntów nienasyconych,* Warszawa: Wydawnictwo Naukowe PWN, 1998.

[12] PN-EN 1997-1, *Eurokod 7 Projektowanie geotechniczne. Część 1: Zasady ogólne.*

INFLUENCE OF NON-ENZYMATIC POST-TRANSLATIONAL MODIFICATION OF HISTONES IN THE AORTIC CELLS ON ATHEROSCLEROSIS - PRELIMINARY STUDIES

Aleksandra Kuzan[1*], Diana Indyk[1], Karolina Nowakowska[2], Katarzyna Rajtczak-Wielgomas[3]

[1] Katedra i Zakład Biochemii Lekarskiej, Wydział Lekarski, Uniwersytet Medyczny im. Piastów Śląskich, Wrocław
[2] Katedra i Zakład Fizjologii, Wydział Lekarski, Uniwersytet Medyczny im. Piastów Śląskich, Wrocław
[3] Katedra i Zakład Histologii i Embriologii, Wydział Lekarski, Uniwersytet Medyczny im. Piastów Śląskich, Wrocław
* corresponding author: aleksandra.kuzan@umed.wroc.pl

Abstract:

It is postulated that histone proteins are susceptible to glycation. This process is one of post-translational modification, but unlike others, it is a non-enzymatic process. Modifications can potentially alter gene expression as epigenetic regulation. This research focuses on the role of histone glycation in the walls of blood vessels. It is postulated that this process may influence the expression of proinflammatory, pro-apoptotic or other proteins involved in atherogenesis. The research material were sections of human aortas. The methods were immunohistochemical method using ABC system and fluorescent markers. The results indicate that glycation occurs in the artery walls in intima, media and adventitia, AGE co-locates clearly with the matrix proteins, and the intensity of the immunohistochemical reaction is associated with the degree of atherosclerosis. Co-localization of AGE with nuclei stained with DAPI it's almost not visible. Due to potential therapeutic implications research should be continued.

Keywords:

histones, glycation, atherosclerosis, immunohistiochemical reaction

Introduction

Histones are small (under 23 kDa) alkaline proteins, which together with DNA, are the major chromatin timber. The basic unit of chromatin is the nucleosome created by the histone octamer (two molecules in each H2A, H2B, H3 i H4) and a double helix of DNA wound on it. Between the nucleosomes there are segments of the spacer DNA to which histone H1 binds. Histones may also include histone H2A variants, such as: H2AX, H2A.Z; H2A.Bbd or macroH2A [1].

Histones contain a non-polar globular domain, also called histone fold, inside the histone octamer and N-terminal domain, rich in basic amino acids, especially the arginine (R) and lysine (K) residues, giving a polar character. The N-terminal part that is extended beyond the histone core as well as the globular domains of histone proteins and non-histone proteins can undergo post-translational modifications, e.g. methylation (me), acetylation (ac) and phosphorylation (ph), ubiquitination, sumoylation, ADP-ribosylation, propionylation, biotinylation [1-4].

Mechanisms that affect the change in genetic expression and do not result from the change in the DNA sequence are called epigenetic mechanisms. Modifications of histones through chromatin condensation / decondensation may affect the expression of genes, either for the activation or repression of gene expression depending on the type of the attached functional group and the type of amino acid residue that undergoes modification. It is speculated that changes in histone modification are one of the factors promoting cancer transformation, especially acetylation or methylation [1, 5]. Less numerous, but there are also papers focusing on the covalent modification of histones that cause neurological diseases [2].

This paper concerns a specific post-translational modification, because unlike the rest, it is non-enzymatic. It is based on the reaction of reducing sugars (glucose, fructose, glucose-6-phosphate and others) or carbonyl compounds (3-Deoxyglucosone, methylglyoxal, glyoxal and others) with amino groups, mainly amino acids lysine and arginine, less frequently histidine. This process is called glycation and leads to advanced glycation end products (AGE) production. Glycation is a multi-stage process. The first stage is the formation of the Schiff base by the interaction of the free amino group (especially lysine) with the carbonyl group of the sugar. Then alters Amadori rearrangement and enaminol is formed. The reactions are reversible to this stage, the next – the formation of ketoamine – is irreversible. Then Maillard reactions take place involving different transformations of the oxidation type, dehydration, fragmentation, condensation with other amino groups, resulting in the formation of appropriate AGE [6,7], e.g. furooyl furanyl-imidazole (FFI), carboxymethyllysine (CML), carboxyethylolysine, piraline, pentosidine [8,9]. Glycation is a relatively slow process that occurs depending on the conditions (temperature, pH, concentration and types of substrates) over days, weeks or even months, hence it mainly concerns proteins with a long half-life [10]. Histones are characterized by a relatively long half-life (4-5 months). Other features of these proteins – that they are small and they have a lot of basic amino acids also predisposes histones to glycation [11].

In patients with diabetes, glycation is intensified for the increased concentration of sugars that are the substrate of the process. Therefore, the glycation of various proteins, including histones, is mainly described in the context of diabetes [12], sometimes it is also analyzed in relation to cancers [5]. In the literature on the subject, there is no well-established knowledge about the effect of glycation of histones found in myocytes and endothelial cells of the blood vessel walls on the development of atherosclerosis.

The aim of this research is to determine whether there is a colocalization of histones and advanced glycation end products and whether there is a relationship between the intensity of labeled products of glycation and the severity of atherosclerosis.

Materials and methods

The research material were fragments of 14 aortas of people who died with sudden death.

Immunohistochemical method

Standard immunoenzymatic reactions were carried out using the ABC method (Avidin-Biotin Complex) using the Mouse and Rabbit Specific HRP / DAB kit (ABC) Detection IHC Kit (Abcam) as well as monoclonal mouse anti-AGE antibodies (Biomatic) and goat polyclonal anti-mouse antibodies with Alexa Fluor® 488 (Abcam). The procedure was carried out analogously

as described in Kuzan and colleagues [13]. The classic immunohistochemical preparations were closed with Mounting medium DPX (POCH) and the fluorescent preparations were closed with Fluoroshield mounting medium with DAPI (Abcam).

Results

Immunohistochemical experiments indicate that there is an AGE antigen in the aortic walls. In the analyzed samples at low stage of atherosclerosis, antigen concentration occurred in adventitia and intima (Fig. 1). In cases where myocytes migrate and proliferate, the concentration of antigen in the media is also observed (Figure 2). It seems that there is a dependence of intensity of immunohistochemical reaction on the severity of atherosclerosis. Nevertheless, the colocalization of the antigen with the cell nucleus is not noticeable. Both types of staining (Figures 1, 2 and 3) indicate that AGEs are most often created along the fibers of the extracellular matrix, hence its presence mainly in adventitia (Fig. 1). Interestingly, the concentration of AGE on the endothelium is not observed, where, according to the classical theory of atherogenesis, the formation of atherosclerotic plaques originates. Relatively a lot of antigen is observed in the area of fat cells (Figures 2 and 3).

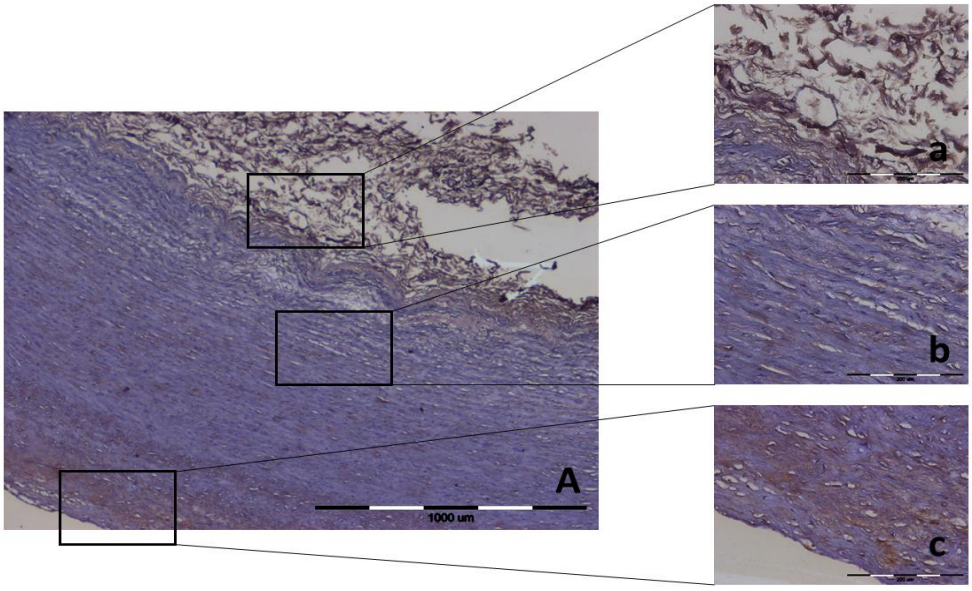

Figure 1. Microphotography of aortic preparation at low stage of atherosclerosis after immunohistochemical reaction using anti-AGE antibodies (ABC method) with differential staining of basophilic structures with hematoxylin. Panel A - cross-section through the wall of the vessel, panel a - adventitia, panel b-media, panel c -intima. Panel A- magnification 40x, panel a, b, c - magnification 200x.
Source: own photo

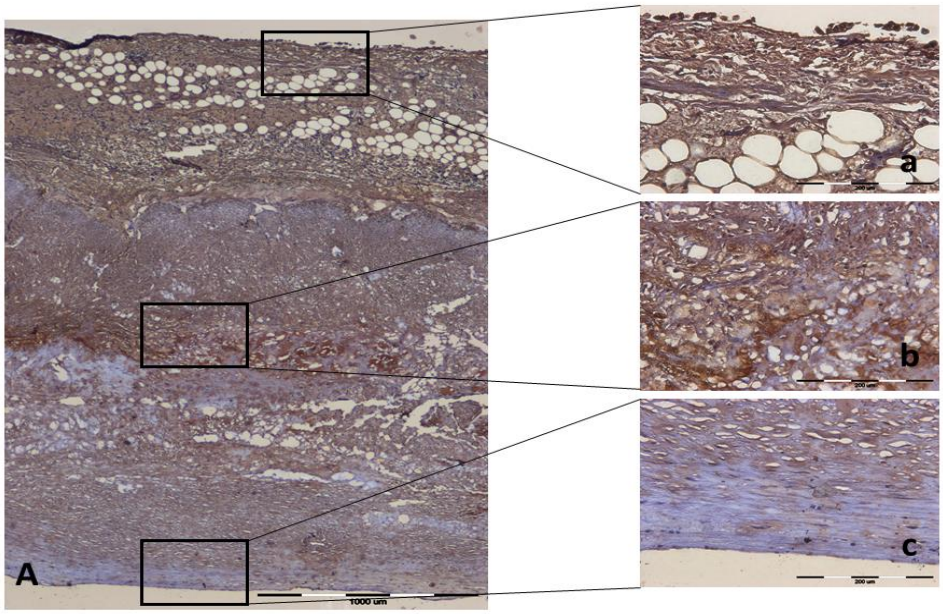

Figure 2. Microphotography of aortic preparation at the intermediate stage of atherosclerosis after immunohistochemical reaction using anti-AGE antibodies (ABC method) with differential staining of basophilic structures with hematoxylin. Panel A - cross-section through the vessel wall, panel a - adventitia with fat cells, b-media panel, c -intima panel. Panel A- magnification. 40x, panel a, b, c - magnification 200x.
Source: own photo

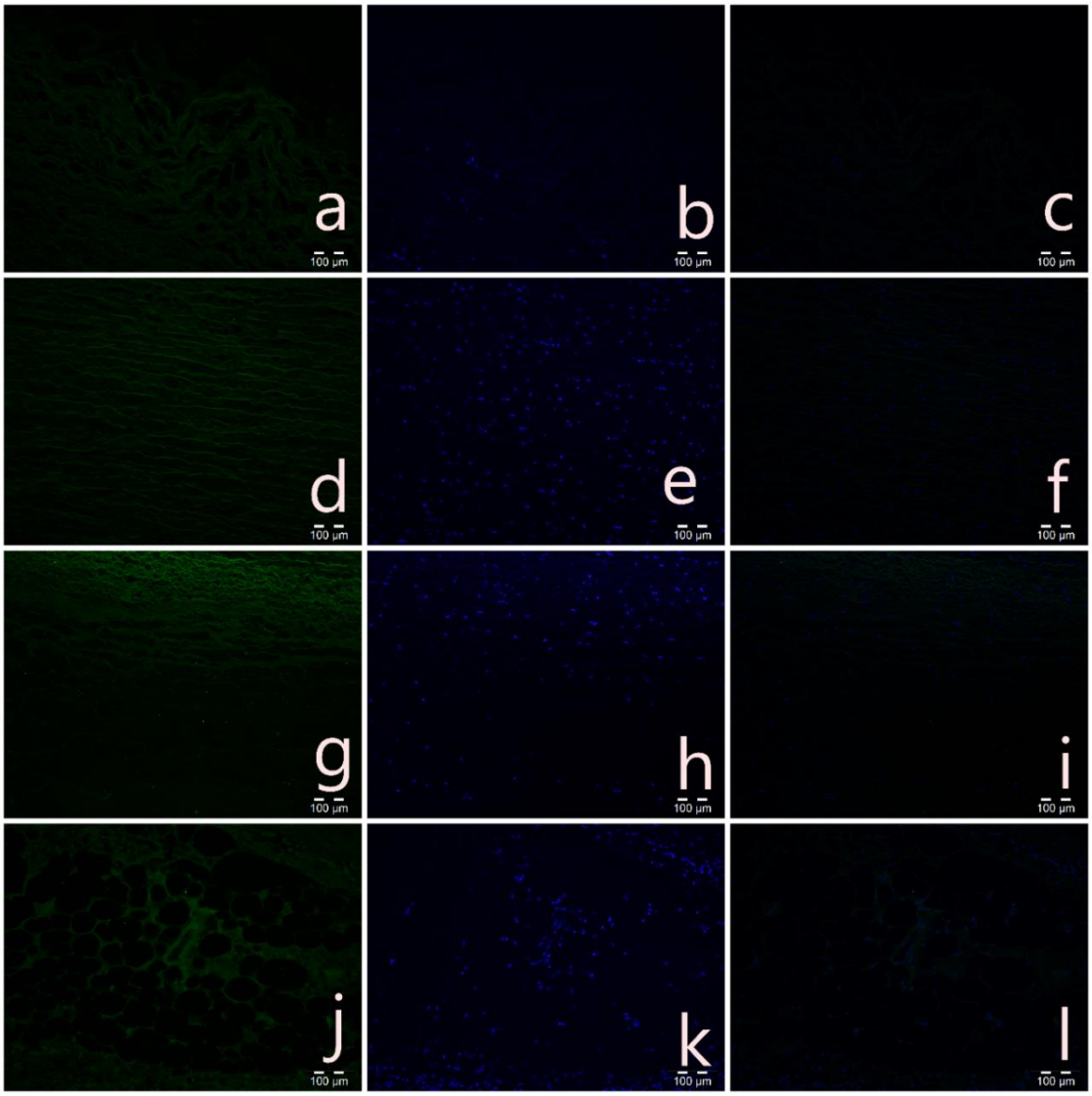

Figure 3. Microphotography of the aorta preparation after the immunohistochemical reaction using anti-AGE antibodies (+ secondary antibody from Alexa Fluor488) (panel a, d, g, j), stained cell nuclei with DAPI (panel b, e, h, k), image overlay (panel c, f, i, l). Adventitia (panel a, b, c), media (panel d, e, f), intima (g, h, i), fat cells in adventitia (panel j, k, l).
Source: own photo

Discussion

It is proven that accumulation of AGEs is related to the pathology of various disorders including diabetes, cancer, chronic inflammation, arthritis, Alzheimer's disease, arteriosclerosis, myocardial hypertrophy and dialysis amyloidosis [14]. However it is not explained which proteins are modified by glycation and what is the effect of structural changes in individual proteins on the course of pathology.

In the 90s of the last century, scientific work began to appear demonstrating the presence of AGE in atherosclerotic plaques using specific antibodies. One of the first teams to deal with this was Nakamura et al. who stained AGE in the arteries using non-commercial anti-AGE-RNAase polyclonal antibodies, while observing the presence of AGE in the extracellular matrix, with particular intensity in samples from diabetics [15]. Stitt et al. showed that in non-diabetic

subjects, AGE compounds are localized in atherosclerotic lesions. Interestingly, in the early and the highest stage of atherosclerotic plaques, accumulation of antigen was seen extracellularly, whereas in intermediate-level plaques AGE were localized intracellularly, in SMC and macrophages containing fats. It can be expected that the staining at least in these early stages are associated with collagen or other matrix proteins [16].

The results of these tests are consistent with the results of Nakamura and Stitt. The accumulation of antigen was particularly visible in atherosclerotic plaques, in the proliferation and migration of myocytes and in the area infiltrated by macrophages, as well as in regions with high integrity of extracellular matrix proteins.

As stated in the introduction, the nitrogen substitutes of Lys, Arg, and His residues and the N-terminus of proteins are readily glycated. Histones are basic proteins with a high content of the above-mentioned amino acids, hence it is logical that they are potentially very susceptible to glycation. The expected result in the case of such a designed study was the observation of antigen concentration at the nucleus site, i.e. at the site to which DAPI binds or intensively stained with hematoxylin. The lack of such images of preparations is not conclusive evidence that histone glycation does not affect the development of atherosclerotic lesions, but only indicates that the chosen method is not sensitive enough.

In the literature of the subject, there is no experience directly proving or denying the hypothesis of this work. There are reports based on in vitro tests that show that histones are glycated, e.g. Gugliucci has shown formation of pentosidine and AGE on histones, and Cervantes-Laurean has shown that histones are glycosylated by ADP-ribose [17,18], Talaz and co-workers that H1 histones, core histones or total histones are glycosylated by several sugars (glucose, ribose and fructose) [19]. There are also papers describing the influence of AGE on atherogenesis, e.g. Koike proves that AGEs induce apoptosis of vascular smooth muscle cells, which implies vascular calcification [14]. In addition, AGE, by combining with its receptors (RAGE, scavenging receptors and others), activates many metabolic pathways. The combination of AGE and RAGE results in the activation of NADPH oxidase, which induces oxidative stress and induction of inflammatory processes in the arterial walls, activation of macrophages and platelets, stimulates chemotaxis and leads to an increase in the number of adhesion proteins (mainly VCAM-1, vascular cell adhesion molecule), which results in atherosclerotic plaque hyperplasia and thrombosis [7,20,21].

It can be seen that the glycation-histone phenomena and glycation-atherosclerosis are associated, however, the juxtaposition of these three concepts is not analyzed according to the authors' knowledge. It seems that it should be, if glycation can be inhibited, so the answers to the questions asked here can potentially help in the treatment of this major civilization disease.

Limitations of the Study: A certain problem is the autofluorescence of proteins that cannot be completely eliminated (despite the implementation of appropriate negative control and prolonged blocking in several blocking solutions). The second limitation is the lack of data on whether the tissue donor had diabetes or not. The limiting factor was also the low number of samples and one type of anti-AGE antibody that was not defined. The continuation of the study assumes testing on a larger number of samples and using other anti-AGE monoclonal antibodies, eg anti-CML or anti-pentosidine.

The work was finalized by the National Science Center (decision number DEC 2017/01 / X / NZ9 / 00599).

Literature

[1] P. Gomulak, J. Blasiak, *The significance of histone modifications in malignant transformation*, Postępy biochemii, (2012), Vol 58(3), 292-301.
[2] B. M. Gruber, *Epigenetics and etiology of neurodegenerative diseases*, Postępy Higieny I Medycyny Doświadczalnej, (2011), Vol. 65, 542-51.
[3] Y. Chen, R. Sprung, Y. Tang, H. Ball, B. Sangras, S. C. Kim, et al., *Lysine propionylation and butyrylation are novel post-translational modifications in histones*, Molecular & Cellular Proteomics, (2007), Vol. 6(5), 812-9.
[4] T. Kouzarides, *Chromatin modifications and their function*, Cell, (2007). Vol. 128(4), 693-705.
[5] P. J. Thornalley, *Protecting the genome: defence against nucleotide glycation and emerging role of glyoxalase I overexpression in multidrug resistance in cancer chemotherapy*, Biochemical Society Transactions, (2003), Vol. 31, 1372-1377.
[6] A. Jabłońska-Trypuć, R. Czerpak, *The role of non-enzymatic glycosylation of proteins in ageing processes and pathogenesis of geriatric diseases*, Postępy Biologii Komórki, (2007), Vol. 34(4), 683-693.
[7] J. Pietkiewicz, E. Seweryn, A. Bartys, A. Gamian, *Receptors for advanced glycation end products and their physiological and clinical significance,* Postępy Higieny I Medycyny Doświadczalnej (2008), Vol. 62, 511-523.
[8] D. A. Slatter, N. C. Avery, A. J. Bailey, *Collagen in its fibrillar state is protected from glycation*, International Journal of Biochemistry & Cell Biology, (2008), Vol. 40(10), 2253-63.
[9] M. Warwas, A. Piwowar, G. Kopiec *Zaawansowane produkty glikacji (AGE) w organizmie – powstawanie, losy, interakcja z receptorami i jej następstwa*. Farmakopeja Polska, (2010), Vol. 66, 585-590.
[10] A. Kuzan, A. Chwiłkowska, M. Kobielarz, C. Pezowicz, A. Gamian, *Glycation of extracellular matrix proteins and its role in atherosclerosis,* Postępy Higieny I Medycyny Doświadczalnej, (2012), Vol. 66, 804-809.
[11] J. M. Ashraf, G. Rabbani, S. Ahmad, Q. Hasan, R. H. Khan, K. Alam, et al., *Glycation of H1 Histone by 3-Deoxyglucosone: Effects on Protein Structure and Generation of Different Advanced Glycation End Products*, Plos One, (2015), Vol. 10(6), 15.
[12] N. A. Ansari, D. Dash, *Biochemical Studies on Methylglyoxal-Mediated Glycated Histones: Implications for Presence of Serum Antibodies against the Glycated Histones in Patients with Type 1 Diabetes Mellitus*, ISRN biochemistry, (2013), Vol. 2013, 1-5.
[13] A. Kuzan, A. Chwilkowska A, C. Pezowicz, W. Witkiewicz, A. Gamian, K. Maksymowicz, et al., *The content of collagen type II in human arteries is correlated with the stage of atherosclerosis and calcification foci*, Cardiovascular Pathology, (2017), Vol. 28, 21-27.
[14] S. Koike, S. Yano, S. Tanaka, A. M. Sheikh, A. Nagai, T. Sugimoto, *Advanced*

Glycation End-Products Induce Apoptosis of Vascular Smooth Muscle Cells: A Mechanism for Vascular Calcification, International Journal of Molecular Sciences, (2016), Vol.17(9), 14.

[15] Y. Nakamura, Y. Horii, T. Nishino, H. Shiiki, Y. Sakaguchi, T. Kagoshima, et al., *Immunohistochemical localization of advanced glycosylation enproducts in coronary atheroma and cardiac tissue in diabetes- mellitus*, American Journal of Pathology, (1993), Vol. 143(6), 1649-1956.

[16] A. W. Stitt, C. J. He, S. Friedman, L. Scher, P. Rossi, L. Ong, et al., *Elevated AGE-Modified ApoB in sera of euglycemic, normolipidemic patients with atherosclerosis: Relationship to tissue AGEs,* Molecular Medicine, (1997), Vol. 3(9), 617-627.

[17] A. Gugliucci, *Advanced glycation of rat-liver histone octamers – an in-vitro study*, Biochemical and Biophysical Research Communications, (1994), Vol. 203(1), 588-593.

[18] C. Luevano-Contreras , A. Gomez-Ojeda, M. H. Macias-Cervantes, M. E. Garay-Sevilla, *Dietary Advanced Glycation End Products and Cardiometabolic Risk*, Current Diabetes Reports, (2017), Vol. 17(8), 11.

[19] H. Talasz, S. Wasserer, B. Puschendorf, *Nonenzymatic glycation of histones in vitro and in vivo*, Journal of Cellular Biochemistry, (2002), Vol. 85(1), 24-34.

[20] S. Yamagishi, *Role of advanced glycation end products (AGEs) and receptor for AGEs (RAGE) in vascular damage in diabetes,* Experimental Gerontology, (2011), Vol. 46(4), 217-224.

[21] N. C. Avery, A. J. Bailey, *The effects of the Maillard reaction on the physical properties and cell interactions of collagen*, Pathologie Biologie, (2006), Vol. 54(7), 387-95.

DESIGNED AND ACTUAL FRAME GEOMETRY COMPARISON OF ELECTRIC MOTORCYCLE LEM THUNDER

Kacper Leszczyński[1*], Wojciech Pawlak[2], Piotr Konieczny[3]

[1]Department of Maintenance and Operation of Logistics, Transportation and Hydraulic Systems, Faculty of Mechanical Engineering, Wrocław University of Science and Technology, Wrocław
[2]Department of Fundamentals of Machine Design and Tribology, Faculty of Mechanical Engineering, Wrocław University of Science and Technology, Wrocław
[3]Department of Biomedical Engineering, Mechatronics and Theory of Mechanisms, Faculty of Mechanical Engineering, Wrocław University of Science and Technology, Wrocław
* corresponding author: kacper.leszczynski@pwr.edu.pl

Abstract:

The purpose of the lecture is to present the process of motorcycle frame creation and compare a designed structure to a real frame. It will cover issues such as:

1. How to design motorcycle frame?
2. What is Light Electric Motorcycle project?
3. How to make a motorcycle frame?
4. What is the way to check the geometry of the frame?
5. How to compare designed frame and actual frame?

Keywords:

frame, deviation, motorcycle, geometry

Introduction

This article aims to compare designed and scanned geometry of Light Electric Motorcycle Thunder's frame. Motorcycle frame was entirely designed and made by students of research group PiRM of Wrocław University of Science and Technology.

To compare real structure with a CAD design, Thunder's frame was scanned by optical scanner. Next, a CAD model and scanned model were put at each other in computer program to show a geometry deviation.

Light Electric Motorcycle

Light Electric Motorcycle (LEM) is a students' project of student research group PiRM of Wrocław University of Science and Technology. The main purpose of this project is to design and build motorcycle which complies with regulations of student's competition SmartMoto Challenge. The theme of contest in 2018 was Dakar electric motorcycle. The vehicle built to participate in this competition is called LEM Thunder. Tab. 1 shows main parameters of mentioned motorcycle.

Table 1. LEM Thunder main parameters [1]

Power [kW]	30
Max velocity [km/h]	120
Continuous torque [Nm]	290
Mass [kg]	120
Wheel base [mm]	1475

Source: LEM Thunder Design Brief

Designed frame

For the purpose of the LEM Thunder project, a light frame with desired durability was a desired target. In order to obtain such properties, it was decided to use material EN AW 6063 T6 as a main frame profiles and sheets of EN AW 7020 T6 on the most loaded frame sections according to Fig. 1. It is based on structure of previous model – LEM Falcon [1].

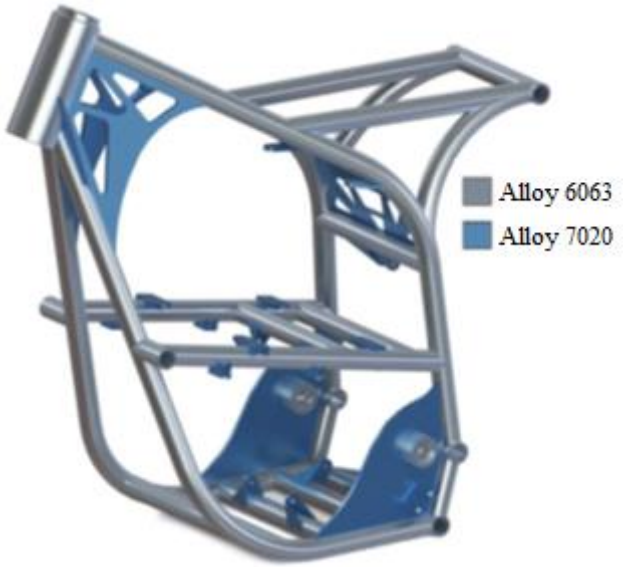

Figure 1. Model of frame with division into different alloy usage [1]
Source: LEM Thunder Design Brief

The safety factor "k" for both materials was set on the level 1,5 which determinate the maximum stress level as 113 MPa for EN AW 6063 T6 and 173 MPa for EN AW 7020 T6 [2][3]. The chassis frame analysis was performed on the shell mode. There were 7 analysis which maximum stress results did not exceed aforementioned values. Mentioned analysis embraced [1]:

- The normal load from maximum carrying mass,
- Acceleration with maximum dynamic case equal 1G and gravity,
- Acceleration with driver standing,
- Emergency braking with maximum dynamic braking force and gravity,
- Emergency braking with driver standing,
- The load from maximum carrying mass using quadruple gravity,
- The load from maximum carrying mass using double gravity with maximum dynamic acceleration equal 1G.

Results of those analysis are shown in Tab. 2.

Table 2. Analysis results [1]

Analysis	Max stress according to Huber-Mises [MPa]
G	30,8
ACC	39,7
ACC DS	87,0
EB	54,5
EB DS	127,7
4G	120,9
2G ACC	129,7

Source: LEM Thunder Design Brief

Final structure weights less than 11kg and fulfill all the strength conditions. Fig. 2 and 3 show LEM Thunder frame with mountings for all of components necessary for motorcycle operation.

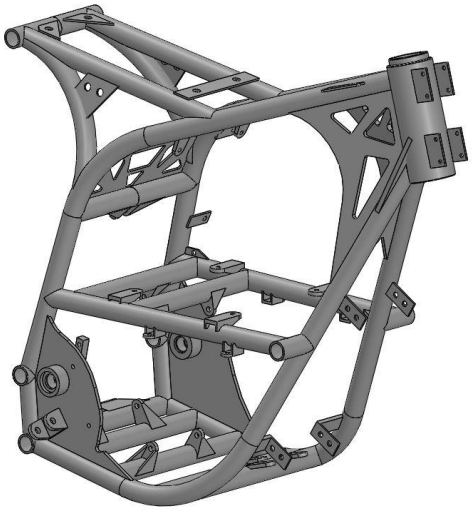

Figure 2. Designed frame model – front
Source: own source

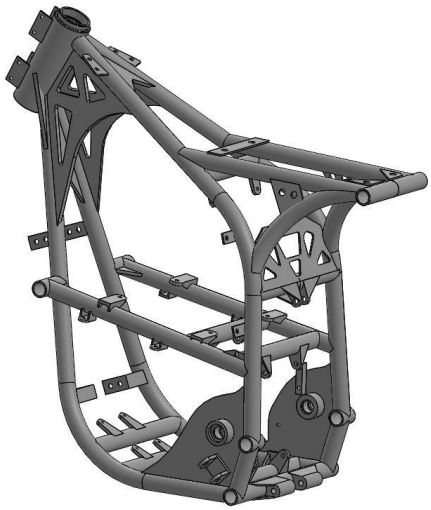

Figure 3. Designed frame model – rear
Source: own source

This type of frame is called double cradle frame. Single cradle frame is simple, basic frame type. It resembles the frame of a bicycle. Double cradle is an evolution of the single cradle, it uses two tubes going down to support the engine on either side. This construction offers better strength and rigidity.

Cradle frames are the simplest of all the motorcycle frames. They are strong and inexpensive to manufacture. For these reasons they are usually found in off-road motorcycles [4].

Actual frame

Making frame stage begins with bending and cutting profiles according to project. Bending took place on a pipe bender and cutting – on water jet cutter.

Before frame welding process there is a need to keep aluminum profiles in the right positions. For the purpose welding station was used. This is a construction made of steel, C-channels and flat bars are cut according to project and fixed with screws. The use of a separable connection allows the frame to be removed after welding. Welding station clearly defines the position of all profiles, which is necessary during welding. Model of welding station with frame is shown in Fig. 4 and 5.

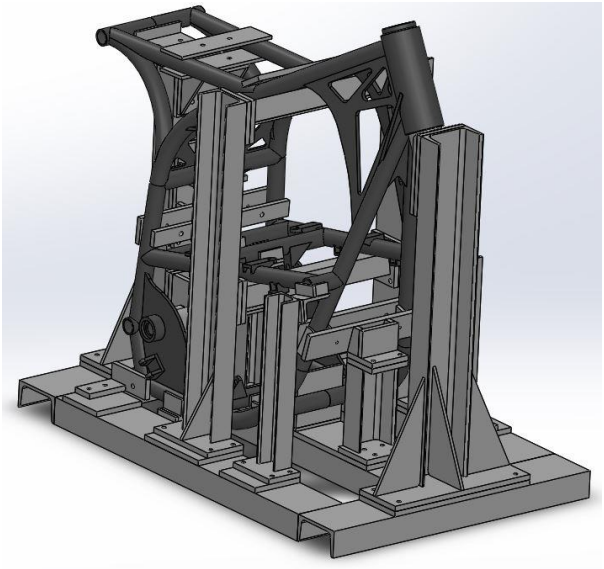

Figure 4. Welding station and frame – front
Source: own source

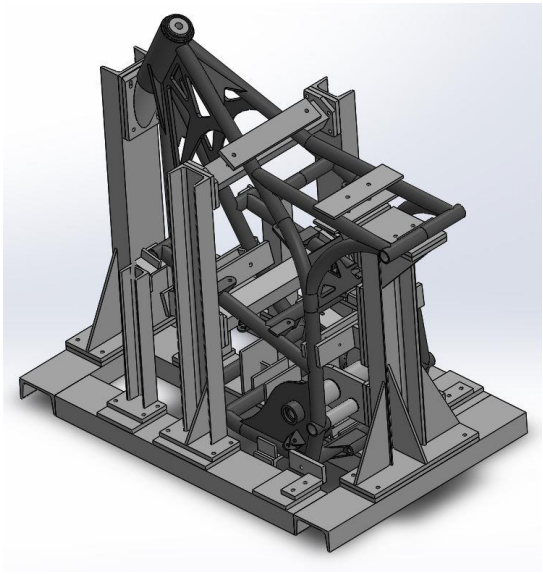

Figure 5. Welding station and frame – rear
Source: own source

The process that was used to connect profiles into a frame is Tungsten Inert Gas (TIG) welding. TIG is an arc welding process. The arc is formed between non-consumable wolfram electrode and welded material. This process was chosen because of pure aluminum welds, which are formed during alternating current welding. The weld area was protected from oxidation and contamination by an inert argon gas I1 according to PN-EN ISO 14175-I1. Filler rod EN-AW-5087 used for welding was 5 mm in diameter. Parameters used for welding are shown in tab. 3.

Table 3. Welding parameters

Max current	AC 200 A
Balance	50/50
Frequency	120 Hz
Gas flow	7,5 l/min

Source: own source

After welding the frame has undergone heat treatment in 150 °C for 7 hours. This process allows to dispose of welding stresses.

Final frame structure was scanned by optical 3D scanner to check its geometry. Actual frame ready to be scanned is shown in Fig. 6.

Figure 6. Actual frame ready to be scanned
Source: own source

Geometry comparison

Points cloud, which is obtained by scanning, was filtered to dispose of noise and then converted into triangulated surface to get surface of scanned frame.

To compare geometry of designed frame and scanned frame, GOM Inspect 2018 program was used. Firstly, CAD model of designed frame and triangulated surface of scanned frame were imported. Then, both models were positioned on headtube, because it defines geometry of the entire frame. It is shown in Fig. 7 and 8, where designed frame is blue and actual is yellow.

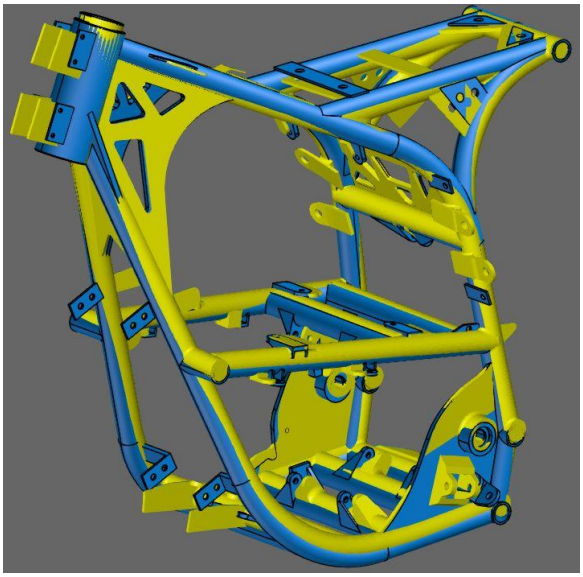

Figure 7. Both model comparison – front
Source: own source

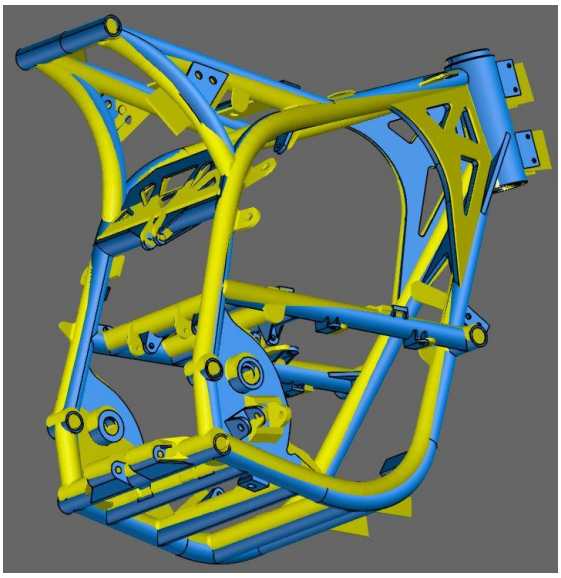

Figure 8. Both model comparison – rear
Source: own source

To get known specific values of deviation the function "surface comparison on CAD" was used. Deviation fields are displayed on designed CAD model. Positives values mean that surface of scanned frame is above designed. Deviation values more than 5 mm and less than -5 mm are marked respectively in pink and black. The limit value of the deviation has been set at 5 mm, because higher values can cause problem with insufficient space for all of components necessary for motorcycle operation. Deviation fields are shown in Fig. 9 and 10.

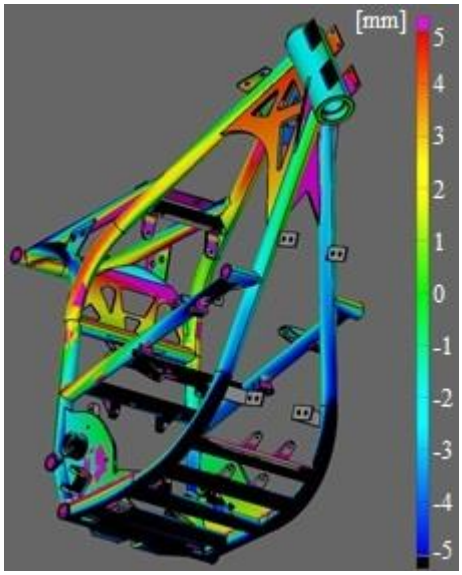

Figure 9. Comparison with deviation – front
Source: own source

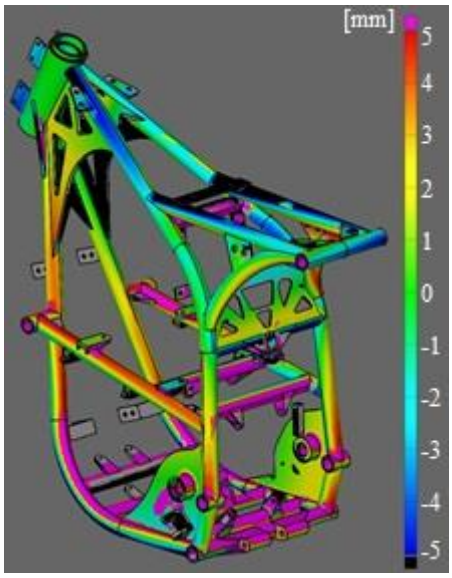

Figure 10. Comparison with deviation – rear
Source: own source

As can be seen the biggest deviation is localized at two main lower pipes. This is due to the fact that bend begins too high compared with designed frame. Each of the lower transverse pipes is out of the limit, because of this error. Other exceeded values are mostly located at mounts, which do not participate in the transmission of stresses. Deviation visible at back upper pipe was created as a result of the error of the welding station.

Summary

Due to the results obtained, it can be concluded that described process of creating the motorcycle frame is correct. The main drawback is precision of workmanship. The best example of this is that deviation of all bottom pipes is caused by wrong cut of main pipes, which was too short. Defects observed in the upper part of the frame are the result of incorrect workmanship of welding station. Profiles prepared to weld were not positioned according to the design.

The quality of described process of creating the frame is acceptable for piece production. However, it is necessary to focus on improving precision of workmanship to make frames whose geometry keeps within tolerance limits.

Literature

[1] Koło Naukowe Pojazdów i Robotów Mobilnych, *LEM Thunder Design Brief*, Wrocław 2018.
[2] *SEBROS Stop aluminium gatunek AW-6063*, http://www.sebros.eu/aluminium/aluminium-EN-AW-6063-ISO:-AlMg0,7Si-EN:-AW-AlMg0,7Si-PN:-PA-38-DIN:---wnr:--/ (access: 30.09.2018)
[3] *SEBROS Stop aluminium gatunek AW-7020*, http://www.sebros.eu/aluminium/aluminium-EN-AW-7020-ISO:-AlZn4,5Mg1-EN:-AW-AlZn4,5Mg1-PN:-PA-47-DIN:-AlZn4,5Mg1-wnr:-3.4335/ (access: 30.09.2018)
[4] Tony Foale, *Motorcycle Handling and Chassis Design: The Art and Science*, second edition, Tony Foale Designs, 2006, ISBN 84-933286-3-4.

THE SPECIFICS OF DEVELOPMENT AND POPULARITY OF STANDARD STAINED GLASS TECHNIQUES IN POLAND IN SECULAR INDIVIDUAL ARCHITECTURE

Marcin Orłowski

Katedra Architektury Mieszkaniowej, Przemysłowej, Wnętrz, Ruralistyki, Krajobrazu i Sztuk Wizualnych, Wydział Architektury, Politechnika Wrocławska, Wrocław
corresponding author: marcin.orlowski@pwr.edu.pl

Abstract:

The article concerns the characteristics of a stained-glass craft available to individual entities unrelated to the Church's institution in Poland in the period after the Second World War (during communism and the centrally planned economy), after the fall of communism (change of economy to free market the beginnings of the Internet) to this day (opening of country borders, development of new technologies and e-economy). Innovation of paper consists in precise indication and characterization of dependencies between periods in Poland and the enormous dynamics of the development of stained-glass craft in the last 30 years since the opening of the country's borders and the advent of the free market and above all the development of the Internet in Poland. These factors influenced the renaissance of stained glass, which is currently the showcase of the country abroad - it overcomes technologically and qualitatively its prototypes.

Keywords:

stained glass, progress, technologies, characteristic, Poland

Introduction

Stained glass windows have always been associated in our aesthetic consciousness with sacred objects, much less frequently with public facilities, palaces and manor houses. They have always aroused the admiration awe of the subject by building the climate, function and rank of the object in architecture (operating in color and value). They owe their prestige not only to the previously described values, but also to the objects in which they were located. These factors were high prices, as well as a small number of craftsmen in relation to other art disciplines. We must also take into account that the next factor was the system and politics - communism, which lasted in Poland in 1945-1989. This system, due to its doctrine, fought against crafts related to the Catholic church. Unfortunately, the first stained glass window was one of those. After the end of the Second World War, the Soviets, when they took over many objects, adapted them to offices and public buildings (and these were mainly manor houses and palaces, which were transformed into office buildings of State Farms, primary schools, commune committees, correctional facilities, etc.). All stained glass windows that were in the window openings were

removed and destroyed. In addition, the People's Government during the Stalinist period repressed the stained glass windows, the purpose of which was to effectively eliminate the craft. After Stalin's death in the 1960s and 1970s, few remaining stained glassworks were treated neglectfully. There was no hand to rebuild this craft or to educate the successors. An additional factor contributing to the decline of the craft was the lack of many raw materials that were not produced in our country or those that were regulated for other industry sectors of those years. The art colleges of that times did not educate in this discipline either, as is the case today. The whole point of the task was to make it difficult for the Catholic Church to obtain contractors in this industry which despite many formal opposition from the central authorities pushed and implemented sacred buildings against objections. The best-known example of such a sabotage action against the authorities of that times was to build a church in Nowa Huta. Such factors were also translated into an average citizen who could not freely order restoration or perform individual order for the needs in a house or flat. The beginning of the 1980s and the era of Jaruzelski's rule introduced a deficit of all goods in the country, rationing on the large scale and a system of card product allocations. It also had a bearing on the stained glass and glass industry. Most of the new block of flats made of the large slab prefabricated building were delivered according to new building standards, according to which the bathroom door had to have gravitational ventilation openings, as well as a window opening to light the bathrooms, as well as a potential gas outlet when the installation leaked or constituted a safety feature that would enable the emergency services to get in the moment of unconsciousness of the user inside due to carbon monoxide poisoning. The solution was very good in its assumptions. Unfortunately, due to economic difficulties, the ornamental glass panes that were supposed to be there were unobtainable (they were often replaced with transparent glazing or if they could be obtained, they were often crushed or damaged as a result of exploitation or damaged by children and youth). There was also a problem in the facilities where the bathrooms had window openings. Mostly these were pre-war objects or from the 1950s and 1960s. At that time, there were only two solutions: painting with paint (mostly oil), or installing curtains / blinds. Both of these solutions were hideous visually and unsightly. When the matter gained a wider range and was formally classed by the Delegations' City of Designs, Voivodeship Committees in Poland, in the late 1980s, a commercially available self-adhesive foil veneer imitating the Chartres stained glass window appeared. It was also the first in history and the last form of stained glass (imitation) proclaimed, allowed for wide circulation by the central authorities. The development of the craft and the whole stained-glass industry was brought about in1989 when communism in Poland fell and consequently also the Iron Curtain, thanks to which the free market economy came into the country. The inflow of literature, magazines and audiovisual materials to Poland has contributed to the increase of knowledge in the field of movements, trends, assortments and technological facilities in the world. In addition, the first specialized stained-glass shops in Poland began to appear. Examples of the first in the country were: Tiffany Glass Center - Kortex in Gdańsk and Arts & Hobby opened in Warsaw. They have in their offer a wide range of raw materials such as: chemicals (acids, patinas), Tiffany soldering tin, ready-made lead profiles, fillers, parts for production of Tiffany lamps, and above all, a rich collection of glass (spectral, cathedral, baola[1], ornament, wissmach, spectrum and many others), With time, in addition to the above, there were also professional courses of varying degrees of advancement, enabling the acquisition

of qualifications necessary for the independent implementation of stained glass. At the beginning of this profession they were teaching craftsmen from Western countries, as well as craftsmen from Ukraine, where this type of creativity, despite socialism, was taught at art academies and also used in socialist architecture as a propaganda tool; moreover, the country undertook many renovations and renovations, including stained glass supplied from capitalist countries, as well as Comecon, which earned for its motto. Moreover, in this country, due to religious conditions, this type of craft did not pose a threat to socialist policy because this creation resulted from an economic factor and did not have a reflection and a world-view significance.

Stained glass windows as an architectural detail

The first detail of architecture was the copies of table lamps, ceiling lamps, wall lamps and external lamps that were copies of Louis Comfort Tiffany's designs. They have been characterized by a great recognition among recipients up till now. They were a kind of new interior quality in the architecture of those years. They broke with boring, crude, monocoloristic lamps from the PRL period. They introduced into the interior, depending on the pattern and color, the individual climate and defined its character. They were a determinant of the owner's property and style. They were not limited to glass. They could also be made, among others, from stones. After entering the Tiffany Glass Center wholesale market in Gdansk, the first Polish workshops in the Tri-City began to be created, binding copper tape in Tiffany's technology and producing amber lamps. When it comes to external lamps, the most popular types are: pendant lamp, wall mounted lamps, street lamps, as well as pole lamps. Lamps, in particular those especially attached to the façade of the building, as well as those that illuminate the balustrades or terraces, have already played a key role in the reception of the architectural body of the building. They usually had the character of a cube, the side walls of which were filled with a single, multiplied stained glass pattern, bound in steel frames, topped with a sloping steel envelope. Due to the high prices of new lamps of this type, at the beginning of the 90s a large part of the lamps were sold on stock markets and markets and came from exhibitions in Germany where this type of lamp was popular much earlier. Around this period, stained-glass furniture inserts also began to flow into Poland, specifying - depending on the country of origin - milled, transparent, galvanized, ornate lacquered frames (popular in the 1970s and 1980s in Great Britain)), single panes of glass decorated with colored foil patterns, finished with self-adhesive lead (Germany). Manufacturers of furniture fronts saw the need for this type of assortment when customers who wanted to assemble stained-glass inserts that were purchased on the stock market started visiting them in large numbers. The first companies started to be created at that time. In most cases, these were producers of furniture fronts. One of the first companies of this type on the national market was the BOBA company from Elbląg, the Pujan company (competition from the same city). Most of these companies offered a wide range of stained glass imitations realized on a single glass pane using colored self-adhesive foil, bound on the outer edges with a self-adhesive, decorative lead profile. These stained glass windows were characterized by repeatability and the possibility of large-scale production, which positively influenced the attractive price of the finished product. The finished glass could be purchased from PLN 64,35 net [2]. With time, these entities also began to offer patterns imitating sandblasted glass made of

transparent film, as well as stained glass enriched with bevels [3], milled glass, attached to the glass with the help of light-cured adhesives. Later, these stained glass windows in the form of individual glass panes started being installed in the window openings, which began to have a significant impact on the architectural aspect of the building. These stained glass windows were easy to distinguish from their counterparts in the original. Firstly, the film did not fully reflect its glass equivalent. It was sometimes too flat (unlike stained glass, it had no traces of rolling, streaking or texture). Secondly, the color range of the film did not even reflect in part its visual equivalent in reality. Thirdly, the most important thing, after opening the window sash or shelf cabinet door, on the other side, the inner side of the self-adhesive profile could be seen, under which adjacent individual elements of the self-adhesive foil faced each other. Fourth, the intersection of the profiles was bumped. The lead tape, at the place of the intersection, passed one on the other instead of flopping. The techniques mentioned so far until the early 2000s were only half measures. It was difficult to reach the client with a stained glass window. The breakthrough came at a time when widely available Internet appeared in Poland. At that time, the first websites of craftsmen began to appear, displaying their realizations, craftsmanship and a wide range of workshops on a large scale. Then, specialized websites devoted to characterizing particular stained-glass techniques also started to appear. They aimed at enabling potential customers to choose the technique and visual expression that would interest them. In addition, the WWW network has enabled everyone, regardless of their visual qualifications, age and education to learn about trends, patterns, movements and tendencies around the world.

The wealthy people began reaching for this craft in its traditional edition more and more often. Stained glass began to go beyond the walls of sacred buildings. The fillings of individual window openings, partitions and openings in the door were particularly popular. These three types have the most important impact on the architectural reception of the object. Stained glass always creates a relationship with the object in which it is located. It creates a narrative in combination with the details relevant to the architectural interpretation of the object. It is important in the context of architecture that the stained glass creates a coherent relationship with the object in which it is located. This character must be consistent, so that the glass work emphasizes the architect's concept, his or her thoughts and ideas contained in the object. A badly made stained glass window can completely disrupt the perception of the object and its function in relation to the design and architectural forerunner. This aspect is extremely important from the point of view of the issue discussed by us. The vast majority of stained glass is ordered by the owners after a long period of residing in the object. Very rarely, design decisions are consulted with architects which creates the risk mentioned above. The craftsmen themselves do not attach much importance to this issue either. It is essential for them to meet the tastes and needs of the investor. The most popular technique chosen by individual users is Tiffany's technique. Its character coherently fits with modern architecture. This technique allows to a greater extent the implementation of the most demanding designs enriched with large curvatures, fines and the magnitude of small details that are not performed in the aforementioned. Customers can choose between semi-transparent and opaque glass, from which we can distinguish smooth and structural glass. In Poland, there are several types of glass available, such as: Cifart, Wissmach [4], Wissmach Mystic, Spectrum [5], cathedral glass [6], Watterglass W, opal, glass type Jasło [7], Uroboros[8], Antic Volcano, Bullseye [9],Youghioghney [10], chinese glass [11] (the

cheapest on the market and the lowest quality; used in cases when the customer wants to have a stained glass window for the lowest price possible), sandblasted, ornamental [12] and glass for fussing [13]. The customer also has a choice of many weld finishes: brass, copper, black and silver. In addition, this technology enables the implementation of spatial elements, the possibility of milling glasses, installing elements from other materials, such as high carbon steel, brass, copper, precious stones, glass mesh [14] [15], lumps [16], and much more. There are also possibilities to make painted elements that are fixed thermally or with ultraviolet light in this technique, as well as apply imprints on the surface adhesive foil (cut at the connection points with a joint; the finished product is not stable for a long time, though). It is correspondent with the film being placed between two sheets transparent glass, rebating its edges, which ensures high durability due to surface protection, as well as a joint that permanently closes the space, preventing the operation of external physicochemical factors. In addition, the tin weld does not corrode or oxidize. It is possible to install a print on a longer-lasting celluloid instead of a foil. This technique, apart from implementing single flat window inserts, enables the implementation of lamps and equipment details such as: window greenhouses, candlesticks, business card holders / organizers and much more. Thanks to this, it is possible to compose consistently all these architectural elements of the interior with each other, in the same time personalizing the interior coherently and to a full extent.

Another technique in terms of popularity is traditional technology, the so-called I-plated bar. This technique has been used for centuries and has the most traditional expression of all. It is suitable both for modern and historic buildings. Its main limitation is the limited degree of complexity of possible designs. In addition, no visual value to welds can be given. It results from the fact that these welds, due to their physicochemical properties, can be finished only with black patina or left in their natural color. A range of glass available is the same as the earlier technique, however, to not disrupt the visual expression, it would be necessary to use traditional glass of the cathedral type. The customer can specify the finish version of the profiles [17] – type "H" (flat face), type "Hr" (convex face with a cross-section of half of the cylinder). Similarly a range of finishing edge profiles can be chosen, too: type "C" (this is a cylinder with a milled technological groove with internal right angles), type "U" (this is a profile type C, whose walls are all flat), type "Y" (so-called a reinforcing construction profile, has an additional flat wall facing outwards on the opposite side of the technological milling cutter, running along the outside in the middle - forming a Y-shaped cross-section, this element protruding in the stained glass nomenclature is called a fin - it is used to assemble the finished product in a cutter, e.g. a window frame). This technology can also be combined with others, for example: fitting elements into the lead luminaire; it is also possible to combine the Tiffany technique with it - it should be remembered that the outer edges of the finished stained glass in this technique should not be framed with copper tape and not soldered (these planes will be put together) and the joints with profiles should be welded on both sides with the profile. It is also possible to integrate the paintings made on the glass with the use of thermosetting paints manually or by machine in this stained glass window. Gobs and bevels can also be inserted in it.

Summary

In summary, the fall of communism and free market economy have contributed significantly to the development of stained-glass craft in Poland. Thanks to the creation of new specialist wholesalers, the branch experienced a renaissance in the light of the needs of individuals. In addition, it has become widely available to all interested entities. The biggest breakthrough affecting its widespread popularity and application not only in sacral buildings but also public, corporate, private, religious communities of other faiths, homes, residences, villas and individual households was exerted by the Internet. It made it possible to find a suitable craftsman, a quality and price list of the raw material, as well as to get inspired and familiarize oneself with the trends and tendencies prevailing in this industry in the country as well as in the world. Currently, we are dealing with a situation where the only limitation of the entity in the stained glass area is the imagination and financial background.

Literature

[1] *ARTS & HOBBY CENTRUM - Szkło do fusing'u Baoli – lipiec 2016,* http://www.artshobby.pl/download/szklo-baoli-do-fusingu-dodatki-do-zdobienia-szkla.pdf, 19.08.2018
[2] *Cennik firmy Pujan z dnia 7.02.2018*, 14.07.2018
[3] *ARTS & HOBBY CENTRUM – Rega Bevels – grudzień 2011,* http://www.artshobby.pl/download/fazowane-szklo-do-wypelnien-drzwiowych-prod-regalead-anglia-najwiekszy-wybor-w-polsce.pdf, 19.08.2018
[4] *Hurtownia Szkła Witrażowego – Sosnowiec ul. Kosynierów 28 – katalogi: szkło Wissmach,* http://www.hurtszkla.pl/catalog/name/down/1/wissmach, 19.08.2018
[5] *Hurtownia Szkła Witrażowego – Sosnowiec ul. Kosynierów 28 – katalogi: szkło Spectrum,* http://www.hurtszkla.pl/catalog/name/down/1/spectrumglass, 19.08.2018
[6] *ARTS & HOBBY CENTRUM - szkło witrażowe Katedralne,* http://witrazowe.com.pl/pl/c/SZKLO-WITRAZOWE/63/7, 19.08.2018
[7] *Hurtownia Szkła Witrażowego – Sosnowiec ul. Kosynierów 28 – katalogi: szkło Jasło,* http://www.hurtszkla.pl/catalog/name/down/1/jaslo, 19.08.2018
[8] *Hurtownia Szkła Witrażowego – Sosnowiec ul. Kosynierów 28 – katalogi: szkło Uroboros* http://www.hurtszkla.pl/catalog/name/down/1/uroboros, 19.08.2018
[9] *ARTS & HOBBY CENTRUM - szkło witrażowe Bullseye,* http://witrazowe.com.pl/pl/c/SZKLO-WITRAZOWE/63, 19.08.2018
[10] *ARTS & HOBBY CENTRUM - szkło witrażowe Youghioghney,* http://witrazowe.com.pl/pl/c/SZKLO-WITRAZOWE/63/7, 19.08.2018
[11] *Hurtownia Szkła Witrażowego – Sosnowiec ul. Kosynierów 28 – katalogi: szkło Chińskie,* http://www.hurtszkla.pl/catalog/name/down/1/chinskie, 19.08.2018
[12] *ARTS & HOBBY CENTRUM - Szkło ornamentowe – marzec 2012,* http://www.artshobby.pl/download/szklo-ornamentowe-takze-do-witrazy-katalog.pdf, 19.08.2018
[13] *Hurtownia Szkła Witrażowego – Sosnowiec ul. Kosynierów 28 – katalogi: szkło do fusingu,* http://www.hurtszkla.pl/catalog/name/down/1/fusing, 19.08.2018

[14] *Hurtownia Szkła Witrażowego – Sosnowiec ul. Kosynierów 28 – katalogi: oczka szklane,* http://www.hurtszkla.pl/catalog/629/oczka-szklane-spectrum-96-sfs, 19.08.2018
[15] *ARTS & HOBBY CENTRUM - Kulki, oczka - kaboszony i gomółki szklane – lipiec 2016,* http://www.artshobby.pl/download/drobnica-szklana-oczka-gomolki-brylanciki.pdf, 19.08.2018
[16] *Hurtownia Szkła Witrażowego – Sosnowiec ul. Kosynierów 28 – katalogi: gomółki,* http://www.hurtszkla.pl/catalog/518/gomolki, 19.08.2018
[17] *ARTS & HOBBY CENTRUM – Profile – listwy witrażowe – styczeń 2015,* http://www.artshobby.pl/download/profile-olowiane-mosiezne-cynkowe.pdf , 19.08.2018

ELECTRIC MOTORCYCLE'S BATTERY CONSTRUCTION

Wojciech Pawlak[1*], Kacper Leszczyński[2]

[1] Department of Fundamentals of Machine Design and Tribology, Mechanical Department, Wrocław
[2] Department of Maintenance and Operation of Logistics, Mechanical Department, Wrocław
* corresponding author: w.pawlak@pwr.edu.pl

Abstract:

In this article there is presented construction of the battery dedicated for an off-road electric motorcycle. Nowadays with electric vehicles getting into all areas of life, battery construction is crucial for proper functioning of cars, motorcycles etc. This article presents construction solutions, identified errors and failures and proposes improvements for next models of this battery.

Keywords:

battery, electromobility, construction, motorcycle

Introduction

Over the last years, electric vehicles became more and more popular. New and more powerful models started putting bigger and bigger responsibility on the designers. Couple years ago, when most popular electric vehicles on the market were e-bikes, batteries and cells operating on high current were not as desirable as today. Back then simple nickel strips were sufficient to carry currents and withstand the temperature of working Li-Ion cells [Fig. 1].

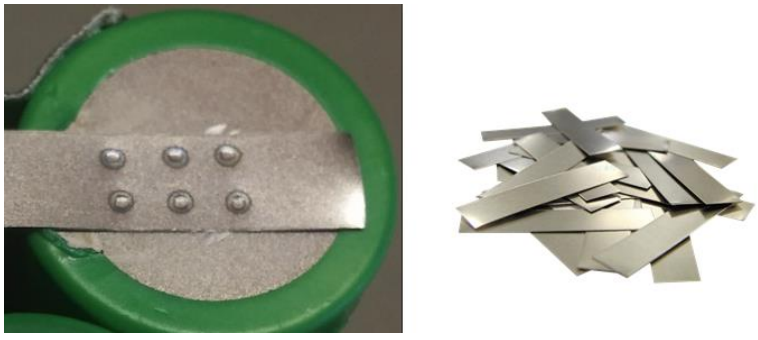

Figure 1. Nickel strips and Li-Ion battery welds
Source: [1]

It is also worth to mention, that Poland in next couple of years will become one of the biggest world Li-Ion cells producer. Due to investments made in Wrocław, up to 3% of world's production will happen in Poland by 2020 [Fig. 2.] [2].

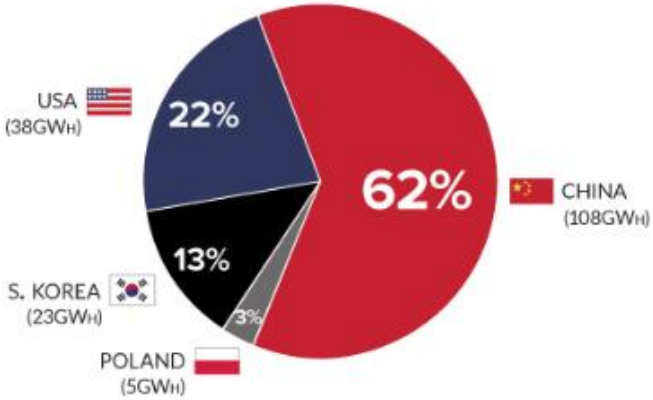

Figure 2. World's Li-Ion production by 2020
Source: [2]

Engineers from the Scientific Association of Mobile Robots and Vehicles build electric motorcycles since 2012. Back then, most of their constructions did not exceed the power of 6 kW [Fig. 3]. Consequently, batteries powering those motorcycles, did not required sophisticated systems of connection and cooling. And therefore whole system was much simpler and cheaper.

Figure 3. Second electric motorcycles built by students of Wrocław University of Science and Technology
Source: own source

But since 2017 these engineers started designing and building much more powerful motorcycles with powers up to 30 kW. Ne construction named LEM Thunder, required battery with configuration 22 cells in series, 20 cells parallel. This configuration with perfect cooling system could power the motor with currents up to 400A.

Figure 4. The newest motorcycle of WUST engineers
Source: own source

LEM Thunder battery construction

Holders

As a core structure for most of the Li-Ion's batteries there are stiff structures called holders. These are the parts that has the purpose of setting in positions all of the cells. Not only for the welding process, but also for the time of using the battery in the vehicle. In this battery model, all of the holders were 3D-printed. For this purpose PLA with carbon fibers enforcement was used, which provided higher thermal resistance. 3D model of a holder is presented in Fig. 5.

Figure 5. Double holder for motorcycle battery
Source: own source

Connectors

As connectors, engineers decided to create custom nickel-copper connectors [Fig. 6.]. Use of standard 0,1 mm thickness nickel strips with customizable thickness of copper plates, in this case 1,5 mm. Nickel strips soldered with copper plates can withstand high currents and temperatures up to 200 °C. In standard conditions, these kind of temperatures are not possible to be achieved in a Li-Ion battery.

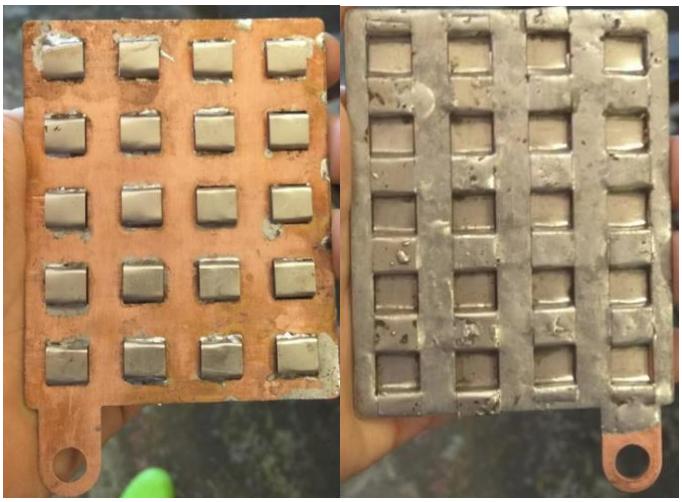

Figure 6. Custom nickel-copper connectors
Source: own source

Case

Strong case for the Li-Ion battery is a must have in an off-road motorcycle. Any failure of case can cause breakdowns of a motorcycle and even explosive effect. For this battery, there was designed and manufactured custom stainless steel case [Fig. 7.]. 1 mm thickness of walls, provided good enough endurance for any possible side hits. Whole inside of the battery was also covered with protective foam [Fig. 8.] and the battery case was mounted in motorcycle on rubber shock absorbers to prevent any long lasting degradation of weldments and soldered connections.

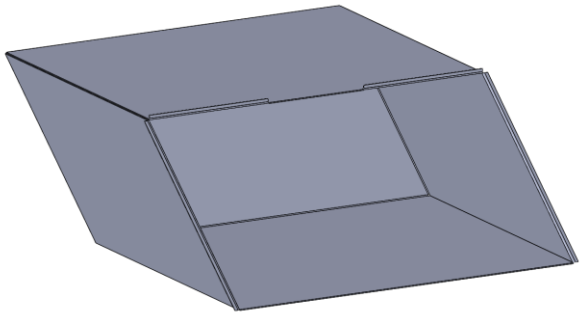

Figure 7. Battery case
Source: own source

Figure 8. Battery case with protective foam
Source: own source

Internal electronic and electric systems

Inside of the battery, there was also a necessity to install Battery Management System, necessary fuses, contactor and radiators for BMS. Despite possible high temperatures of the battery inside it was important to keep power cables as short as possible, due to the safety and power losses reasons.

Assembly

In the Fig. 9, there is presented internal layout of the battery. Most of the battery packs are laid down in the lower part of the battery to keep the center of gravity as low as possible. Main cover also is intended to allow easy access to most crucial electric and electronic parts of a battery for quick fixes and checkups.

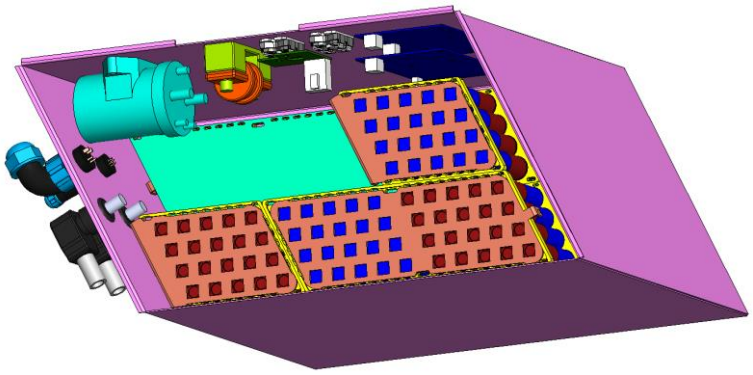

Figure 9. Battery layout
Source: own source

Conclusions

Manufacturing problems and errors

In the process of manufacturing several packs for the battery, there occurred some problems with both welding and soldering connectors and Li-Ion cells. Even with clean soldering machine nozzle, there often formed inhomogeneities and impurities [Fig. 10.]. Later on, these errors can cause higher electric resistance and in consequence problems with proper functioning of a whole system.

Figure 10. Errors during soldering
Source: own source

Due to unevenness of nickel strips in some points, there appeared a problem with proper welding. To get the correct weldment, not only perfectly clean surfaces are needed, but as big as possible contact field of both joining materials. Any disturbance of this condition can cause rising electrical resistance in the point of weldment, and in consequence burnout of one or both materials.

Possible solutions

To avoid above mistakes, there is a need of changing both design and manufacturing technology. As one of a first tries, inexpensive and fast method fulfilled its task, but for more endurable and professional battery it is important to avoid weak spots in those places. To ensure good weldments between connectors and cells, the design should contain rule to make the connectors as flat as possible. Less or even no folds on nickel strips should provide big enough contact field.

Regarding the nickel-copper connection, it is possible to use much more sophisticated technology as ultrasonic welding. Purity of this kind of connections, would greatly improve effectiveness of whole connector production. Exemplary connector is presented in Fig. 11. The nickel inserts are cut through to deliver contact between nickel plate and Li-Ion plate during the welding, when the machine presses the electrodes onto the joined materials.

Figure 11. Exemplary connector

Source: [3]

Literature

[1] Źródło internetowe: *EbikeSchool.com*, http://www.ebikeschool.com/how-to-differ-between-pure-nickel-strip-battery-tabs-vs-steel-core/, 28.09.2018.
[2] Źródło internetowe: *Benchmark Mineral Intelligence*, http://www.visualcapitalist.com/china-leading-charge-lithium-ion-megafactories/, 28.09.2018.
[3] Źródło internetowe: https://www.alibaba.com/product-detail/battery-welding-Connector-Copper-plate-for_60677770382.html, 28.09.2018.

COMPARATIVE ANALYSIS OF THE MOTORCYCLE SUBFRAME MADE OF COMPOSITE MATERIALS

Paweł Stabla*, Paweł Zielonka

Faculty of Mechanical Engineering, Wrocław University of Science and Technology, Wrocław
*corresponding author: stabla.pawel@gmail.com

Abstract:

In this paper a comparison of two motorcycle subframes made of different composite material layups is presented. The first sample is manufactures purely from the carbon and carbon-aramid wovens. The second sample contains additionally a foam core. The elements were tested on a strength machine in order to obtain the curve of force-displacement. Especially dedicated experimental equipment was constructed as well. The tests revealed that the proposed layup including the foam core does significantly decreases the durability of the subframe. Nonetheless, there is a great possibility to improvement, especially in the area of manufacturing the final element. The subframe comes from a prototype motorcycle, so the technology is on ideally optimized. A further work is going to be proceeded.

Key words:

composite materials, electric motorcycle, motorcycle subframe, foam core

Introduction – LEM Falcon project

LEM Falcon (Fig. 1) is a students' project made by the members of Scientific Association of Mobile Robots and Vehicles at Wrocław University of Science and Technology. The group gathers almost 60 students working each year on a new electric motorcycle. The aim of the project is to construct and build a new motorcycle with respect to the rules of the competition in which the team takes part. Since 2013, the group competes in SmartMoto Challenge in Barcelona, where students form different countries faces each other on the track their motorcycles. In the 2017 edition, the main conditions pointed out in the rules [1] were the maximum power up to 8 kW, the maximum nominal voltage up to 60 V and the maximum wheelbase up to 1400 mm.

Figure 1. LEM Falcon
Source: own materials

Actual solutions

A subframe is not always used in the motorcycles. The reason why it occurs in a two-wheeler varies form one company to another. Its general task is to provide the construction for seat while simplifying the geometry of the main frame. Thanks to the subframe, the main frame is less complicated and less stiff. The joints between subframe and the main frame are also a place to decrease the vibrations coming from the engine and the road to the rider. [2]

Moreover, if the subframe is made of more flexible material and design than the rest of the motorcycle, it works somehow like an additional suspension for the rider. The other very important task of the subframe is the mounting for lights and other devices. In combustion engine motorcycles, an exhaust system is often mounted to the subframe. In some cases, especially in off-road motorcycles, this part works also as a rear fender.

A good example of the motorcycle with welded subframe is KTM 390 Duke 2017. KTM is the long-time off-road leader, but also produces a variety of on-road two-wheelers. The subframe in this case welded of tubes and screwed to the main frame.

Composite lamination is a growing subframe fabrication method. It was accelerated by the development of the composite industry. Moreover, the pursuit of weight reduction has forced some companies to turn to that group of materials. In comparison the previous group, composites are much more complicated in fabrication, as well as in modelling and strength analysis. The main advantage of this kind of material application is that it provides a sufficient strength and stiffness while having lower weight.

The next example of cross motorcycle is Husqvarna TC 250. In this case, a carbon fibre reinforced polyamide was used. The volume of the reinforcement was set to 30%. The subframe is made in an advanced injection moulding technique. [3]

Subframes made of plastics are the step between steel frames and composite. It is also a well-developed construction, made of sophisticated plastic materials. However, because of the isotropic material parameters, it cannot be so optimized as the composite ones. Nonetheless, it has an influence on the total mass of the vehicle. Turning to plastic materials in such an extreme application has a positive effect on the development of this group of materials.

Alta Motors is an American company that producer solely electric motorcycles. The material that they used for a subframe is called Makroblend® UT6007. It is a resin consisting of

polycarbonate (PC) and polybutylene terephthalate (PBT). A blend of these two materials gives in result a resin with tensile module 2,2 GPa and tensile strength 60 MPa [4].

Composite materials characteristic

The choice reinforcement type was a result of the possibility of the Association of Vehicles and Mobile Robots. Under the interests were two wovens: carbon, and carbon-aramid (hybrid). Both the materials that were used in the subframe part are the twill woven with plain patterns and 200 GSM. The choice of such a structure was dictated by the good formability in the form while laminating the composite. Although it does not make the full use of fibres properties, it is still worth enough to use.

The second component of the composite material is a matrix. The matrix that was chosen for the investigated subframe was epoxy resin LP470 and the hardener HP403. The team working with composites has the biggest experience with this kind.

In the second subframe, an additional foam core was used with the thickness of 10 mm, Rohacell. The aim of the application of such layer was to check whether it is worth-using in the light of cost and mass parameters of the subframe element.

The layups of the two subframes are presented in the Fig. 2.

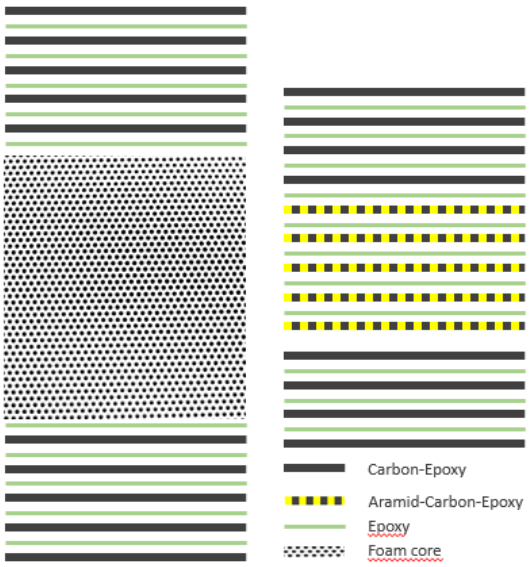

Figure 2. Composite layups from subframe with core and without
Source: own materials

Investigated element

The main aims of the subframe in LEM Falcon motorcycle were to simplify the main frame and to work as a support for the seat. Also, it acts as a rear fender and the mounting area for the rear lights. The design of the subframe was influenced by the technology that it could be manufactured in the students' conditions. For manufacturing such an element, a vacuum bagging technique was used. For that, 3D printed molds were prepared. The design and the final product are presented in the Fig. 3.

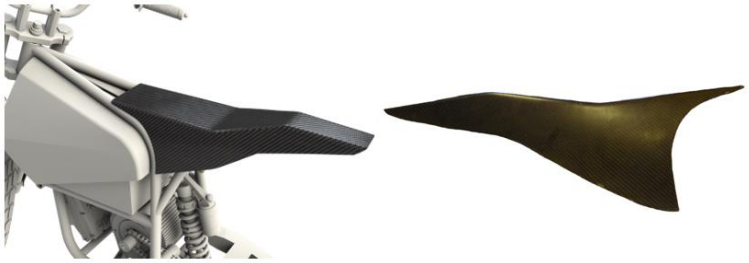

Figure 3. The model and the final element of the subframe
Source: own materials

Methodology and experiment equipment

The main aim of the experiment was to reflect somehow the working conditions of the subframe, but in the static behavior. Therefore, an experiment equipment must have been constructed so that it could reflect the real mounting of the subframe and the loading of the rider. Mounting points can be observed on the Fig. 4.

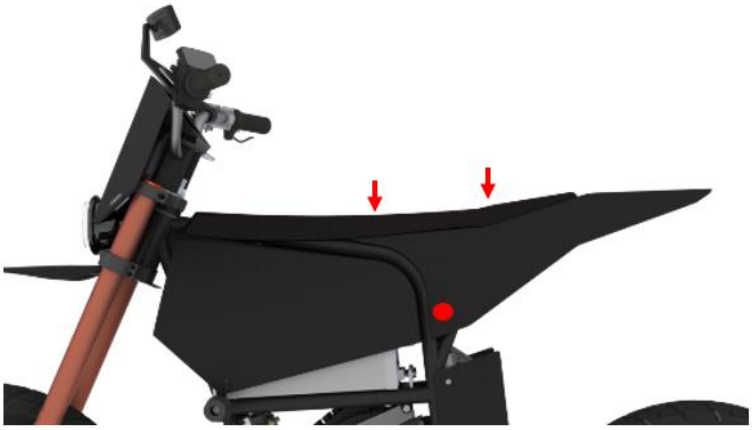

Figure 4. The subframe with pointed mounting points
Source: own materials

In order to eradicate the influence of the deformation of the equipment, a heavy and stiff steel welded elements were used. The final equipment can be seen in the Fig. 5.

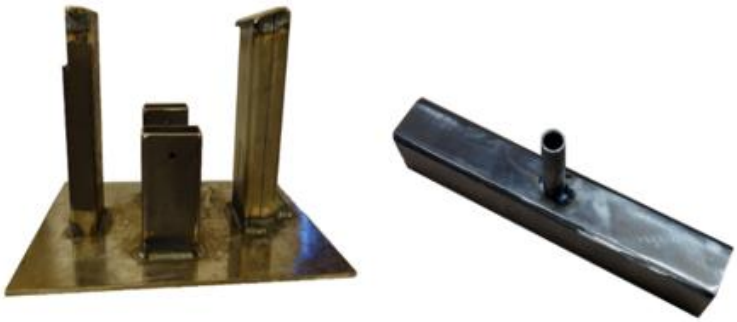

Figure 5. The experimental equipment for the test
Source: own materials

Experiment and results

The original parameters of the test are pointed out in the Table 1. The loading pin speed was set on such a value in order to provide a static behaviour of the test.

Table 1. The parameters of the test

Parameter	Value
Steering	Displacement
Measuring	Force
Loading pin speed	2.5 mm/min
Maximum displacement	20 mm

Source: own materials

The complete test stand was assembled and adjusted so that every part was in a proper position. A considerable attention must have been payed to the position of the loading pin. Especially, the perpendicularity to the symmetry plane of the subframe. The assembly and the test stand are shown in the Fig. 6.

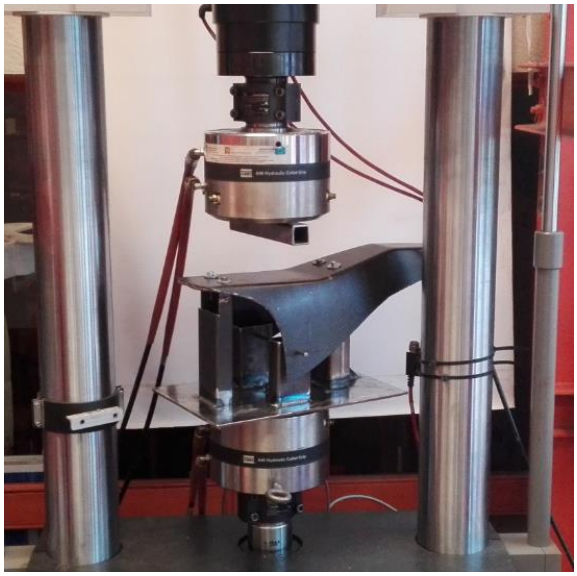

Figure 6. Subframe mounted on the test machine
Source: own materials

After two tests of subframes with different layups, the following curves were obtained and can be seen in the Fig. 7.

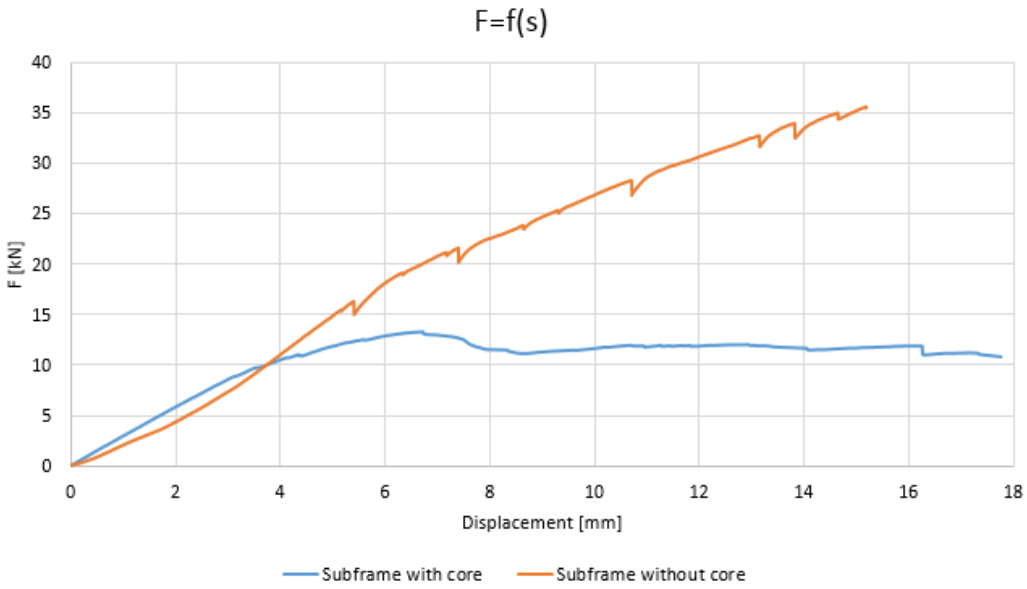

Figure 7. The curves of force-displacement for the particular subframes
Source: own materials

For the subframe without the core, generally, the force is rising with the displacement. The maximum obtained force is 35.6 kN for the displacement of 15.2 mm. For this displacement the experiment was stopped.

Nonetheless, the curve is not constantly rising. A few falls of force occurred during the experiment. It took place at 5.4 mm, 7.4 mm, 10.7 mm and more frequently at the last moments of the experiment. The force falls are approximately at 1.3 kN levels. The reason of these behaviour comes from the construction of the equipment. Namely, the side mountings of the subframe were reflected as a pin going through the holes in the subframe and the equipment. No additional screwing was used. Therefore, during the experiment, some displacement of the subframe in relation to the pin occurred. It is displayed by the falls of the force on the graph below.

For the subframe with the core, the behaviour of the force is quite different. At the first 3 mm, the growth rate of the force is higher than in the second subframe. The force is lower from the displacement of 4 mm. At the level of 6,5 mm, after reaching 13,3 kN, a sudden fall can be observed. Then, the force stabilizes at 12 kN. While reaching 16 mm, another small fall occurs, when one of the side of the subframe cracks. Then, the experiment was finished.

Conclusions

Firstly, both tests were conducted properly and finished after a significant sign of a crack. Taking into account the curves of force-displacement, it is noticeable, that the application of the foam core did not resulted in the improvement of the behaviour of the subframe. The resistance of the subframe with the core was considerably lower, and the process of delamination occurred. While the experiments of the subframe without the core finished after a significant crack. Nevertheless, the subframe with the core seems to be strong enough to withstand the real working conditions.

The composite layups presented in this paper are the first steps of authors into strength test of composite materials. In the future, further investigations are going to be proceeded in order to improve the lamination process, experiment equipment and the final layup of the subframe.

Literature

[1] Źródło internetowe: *SMARTMOTO CHALLENGE (SMC) ASSOCIATION., SMARTMOTO CHALLENGE 2017 Rules 8.0*, 2017*, http://www.smartmotochallenge.org/rules.html, unavailable now.
[2] T. Foale, Motorcycle Handling and Chassis Design, 2002.
[3] Źródło internetowe: http://www.husqvarna-motorcycles.com/motocross/2-stroke/tc-250, 15.09.2018
[4] Źródło internetowe: https://www.plastics.covestro.com/en/Products/Makroblend/ProductList/201305212210/Makroblend-UT6007 15.09.2018

PROMOVENDI

Oferujemy:
– skład i łamanie tekstu,
– wydruk książek abstraktów i monografii z numerem ISBN,
– oprawę graficzną wydruków,
– organizację konferencji,
– pomoc w organizacji konferencji,
– obsługę informatyczną i administracyjną konferencji.